Article

Cell Host & Microbe

# RTP4 Is a Potent IFN-Inducible Anti-flavivirus Effector Engaged in a Host-Virus Arms Race in Bats and Other Mammals

## Graphical Abstract

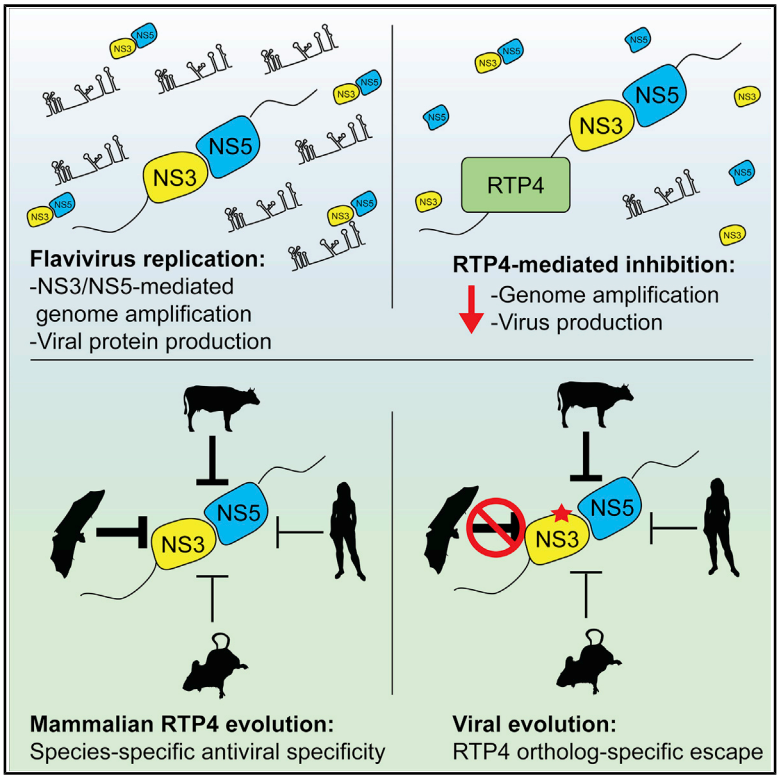


## Highlights

- A screen identifies flying fox RTP4 as an antiviral effector targeting flaviviruses
- RTP4 binds viral RNA and suppresses flavivirus genome amplification
- Mammalian RTP4 orthologs exhibit distinct antiviral properties
- Escape of RTP4-mediated restriction by a flavivirus is ortholog specific

## Authors

Ian N. Boys, Elaine Xu, Katrina B. Mar, Pamela C. De La Cruz-Rivera, Jennifer L. Eitson, Benjamin Moon, John W. Schoggins

## Correspondence

john.schoggins@utsouthwestern.edu

## In Brief

Conflicts between viruses and their hosts drive the evolution of antiviral restriction factors. Boys et al. unveil mammalian RTP4 as an antiviral effector that suppresses the replication of distinct flaviviruses in a species-specific manner, thus highlighting an unappreciated host-pathogen molecular arms race spanning 100 million years of mammalian evolution.

Boys et al., 2021, Cell Host & Microbe *29*, 712–723
November 11, 2021 
https://doi.org/10.1016/j.chom.2020.09.014

CellPress

CellPress

Cell Host & Microbe

Article

# RTP4 Is a Potent IFN-Inducible Anti-flavivirus Effector Engaged in a Host-Virus Arms Race in Bats and Other Mammals

Ian N. Boys,[1] Elaine Xu,[1] Katrina B. Mar,[1] Pamela C. De La Cruz-Rivera,[1] Jennifer L. Eitson,[1] Benjamin Moon,[1] and John W. Schoggins[1,2,*]

[1]Department of Microbiology, University of Texas Southwestern Medical Center, Dallas, TX 75390, USA

[2]Lead Contact

*Correspondence: john.schoggins@utsouthwestern.edu

https://doi.org/10.1016/j.chom.2020.09.014

## SUMMARY

Among mammals, bats are particularly rich in zoonotic viruses, including flaviviruses. Certain bat species can be productively yet asymptomatically infected with viruses that cause overt disease in other species. However, little is known about the antiviral effector repertoire in bats relative to other mammals. Here, we report the black flying fox receptor transporter protein 4 (RTP4) as a potent interferon (IFN)-inducible inhibitor of human pathogens in the *Flaviviridae* family, including Zika, West Nile, and hepatitis C viruses. Mechanistically, RTP4 associates with the flavivirus replicase, binds viral RNA, and suppresses viral genome amplification. Comparative approaches revealed that RTP4 undergoes positive selection, that a flavivirus can mutate to escape RTP4-imposed restriction, and that diverse mammalian RTP4 orthologs exhibit striking patterns of specificity against distinct *Flaviviridae* members. Our findings reveal an antiviral mechanism that has likely adapted over 100 million years of mammalian evolution to accommodate unique host-virus genetic conflicts.

## INTRODUCTION

Host-virus conflicts drive the evolution of antiviral restriction factors, many of which exhibit divergent properties among related species (Daugherty and Malik, 2012). In mammals, a class of antiviral effectors—interferon-stimulated genes (ISGs)—are induced as part of the interferon (IFN) response. The combined activities of ISGs restrict viral infection, but our understanding of the mechanism of action and species specificities of many ISGs is limited. For example, we know the identity, and in some cases the mechanisms, of several human ISGs targeting mosquito-borne flaviviruses (e.g., dengue virus [DENV], yellow fever virus [YFV], West Nile virus [WNV], and Zika virus [ZIKV]) (Li et al., 2013; Richardson et al., 2018; Schoggins et al., 2014, 2011; Suzuki et al., 2016). However, flaviviruses are zoonotic pathogens; they can be transmitted to humans from animals, such as birds or other mammals, frequently via an arthropod vector. We know little about antiviral mechanisms targeting flaviviruses in non-human hosts.

Among mammals, bats are particularly rich in zoonotic viruses, including flaviviruses (Olival et al., 2017). In nature, certain bat species can be productively yet asymptomatically infected with viruses that cause overt disease in other species (Calisher et al., 2006). Of the 1,200+ extant bat species, one of the most studied species from the standpoint of viral zoonoses is the black flying fox, *Pteropus alecto*. It is best known as a reservoir host of henipaviruses (Halpin et al., 2000), though flaviviruses can infect the black flying fox in experimental settings (van den Hurk et al., 2009) and may also naturally circulate in this species (Irving et al., 2020). Experimental studies have demonstrated the ability of the black flying fox to transmit the flavivirus Japanese encephalitis virus (JEV) to mosquitoes, highlighting the species' potential as a reservoir for zoonotic flaviviruses (van den Hurk et al., 2009). Studies of bat immunity suggest that bats have adapted to either tolerate or control viral infection. For example, unique adaptations in immunoregulatory factors that result in decreased inflammation and presumably increased tolerance of viral infection have been described. These include natural killer cell receptors (Pavlovich et al., 2018), components of the inflammasome (Ahn et al., 2019; Zhang et al., 2013), and signaling molecules such as STING (Xie et al., 2018) and IRF3 (Banerjee et al., 2020). Furthermore, studies have revealed both expansion and contraction of IFNs in different bat species (Pavlovich et al., 2018; Zhou et al., 2016). However, efforts to characterize antiviral effector mechanisms in bats are relatively limited. Targeted studies of individual effectors, such as IFITM3 (Benfield et al., 2020) and Mx family GTPases (Fuchs et al., 2017), have yielded insight into unique adaptations in bats. Genome-scale phylogenetic analyses have identified many immune factors (including effectors) that exhibit a signature of positive selection in bats (Hawkins et al., 2019). Otherwise, little is known about the antiviral effector repertoire in bats relative to other mammals.

Here, we screen black flying fox ISGs for their ability to restrict flavivirus infection. We identify and characterize black flying fox

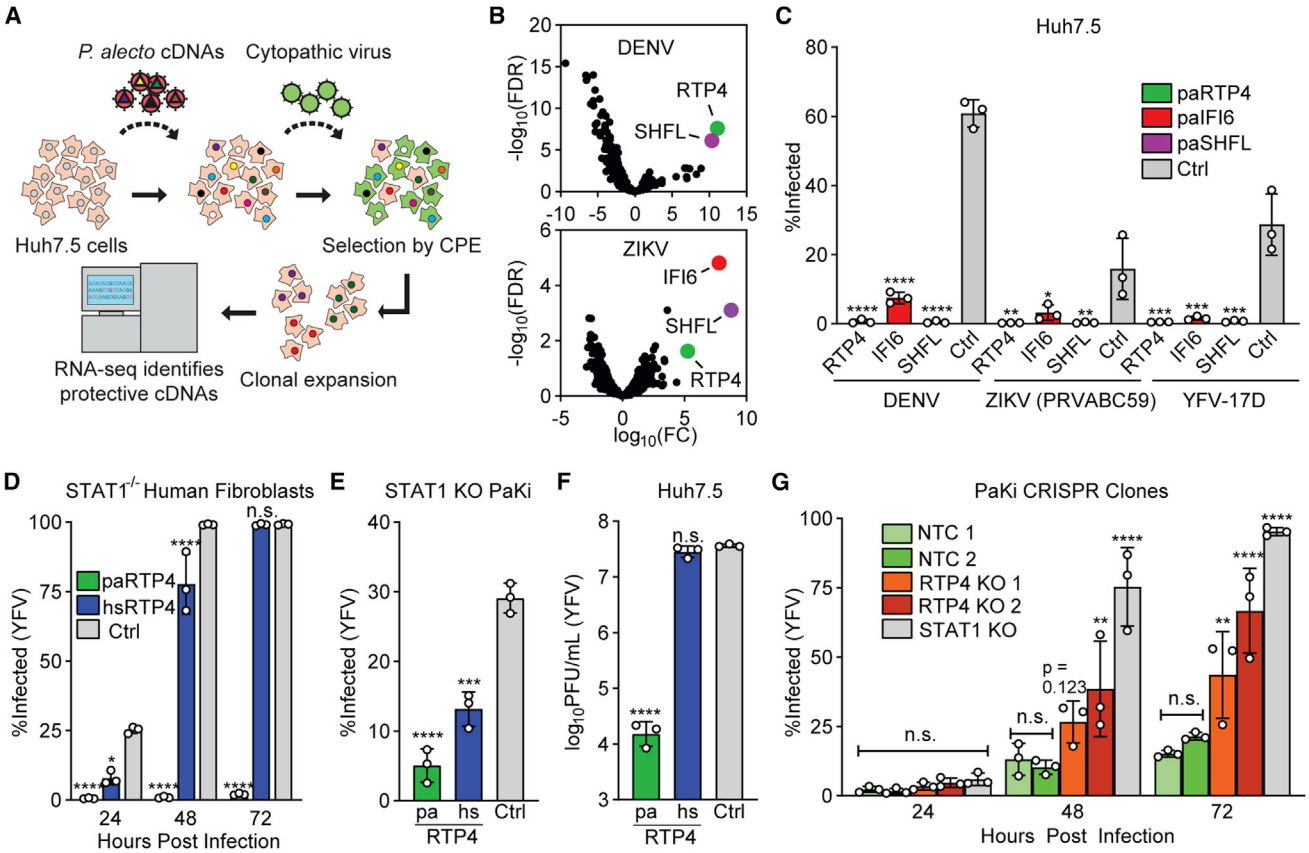


**Figure 1. Black Flying Fox RTP4 Restricts Flavivirus Infection**

(A) cDNA library screening pipeline. See Table S1 and Figure S1A.

(B) Results of triplicate DENV and ZIKV screens. See Data S1.

(C) Huh7.5 cells expressing black flying fox RTP4, IFI6, or SHFL were infected with DENV, ZIKV (PRVABC59), and YFV-17D-Venus (YFV-Venus) for 24 h (YFV, ZIKV) or 48 h (DENV). Bars represent mean ± SD of n = 3 biological replicates. One-way ANOVA with Dunnett's test.

(D) STAT1$^{-/-}$ human fibroblasts transduced with lentiviral pseudo-particles encoding paRTP4, hsRTP4, or firefly luciferase (Fluc) were infected with YFV-Venus for 24, 48, and 72 h. Bars represent mean ± SD of n = 3 biological replicates. Two-way ANOVA with Holm-Sidak test.

(E) AAV-transduced *STAT1* KO PaKi cells were infected with YFV-Venus for 24 h. Bars represent mean ± SD of n = 3 biological replicates. One-way ANOVA with Dunnett's test.

(F) Huh7.5 cells expressing paRTP4, hsRTP4, or a vector control were infected with YFV-17D (MOI of 10) for 24 h. Quantification by plaque assay. Bars represent mean ± SD of n = 3 biological replicates. One-way ANOVA on log-transformed data with Dunnett's test.

(G) CRISPR-*RTP4* KO PaKi clones were infected with YFV-Venus (MOI of 0.05). Bars represent mean ± SD of n = 3 biological replicates. All statistics are relative to NT.1. Two-way ANOVA with Holm-Sidak test.

receptor transporting protein 4 (RTP4) as a potent IFN-inducible effector that suppresses genome amplification. We further assess the antiviral properties of RTP4 from nine diverse mammals and find that each exhibits a striking level of functional specialization across mammalian species. Moreover, the experimental evolution of a flavivirus yielded an adaptation that promotes the escape of inhibition by one RTP4 ortholog but not others, underscoring the specificity of the host-virus molecular arms race.

## RESULTS

### A Gain-of-Function Screen Identifies Black Flying Fox RTP4 as an Inhibitor of Flavivirus Infection

IFN induces ISGs and protects black flying fox cells from viral infection (De La Cruz-Rivera et al., 2018; Zhou et al., 2016). To establish a screening platform to identify these protective genes, we treated kidney-derived black flying fox cells (PaKi cells) (Crameri et al., 2009) with IFN to generate a cDNA library enriched for antiviral ISGs (Figure S1A; Table S1). We expressed the cDNA library in Huh7.5 cells and infected them with DENV and ZIKV. Virus-induced cell death eliminated cells that expressed non-protective cDNAs. Cells that resisted infection, presumably via antiviral gene expression, were expanded, and the enriched bat cDNAs were identified by RNA sequencing (Figure 1A). Three black flying fox ISGs were enriched in cells that survived either DENV (RTP4 and SHFL) or ZIKV (RTP4, shiftless [SHFL], and interferon alpha-inducible protein 6 [IFI6]) infection (Figure 1B; Data S1). We and others have characterized human IFI6 as a flavivirus restriction factor (Dukhovny et al., 2019; Richardson et al., 2018), and human SHFL is a known effector with broad antiviral activity (Balinsky et al., 2017; Suzuki et al., 2016; Wang et al.,

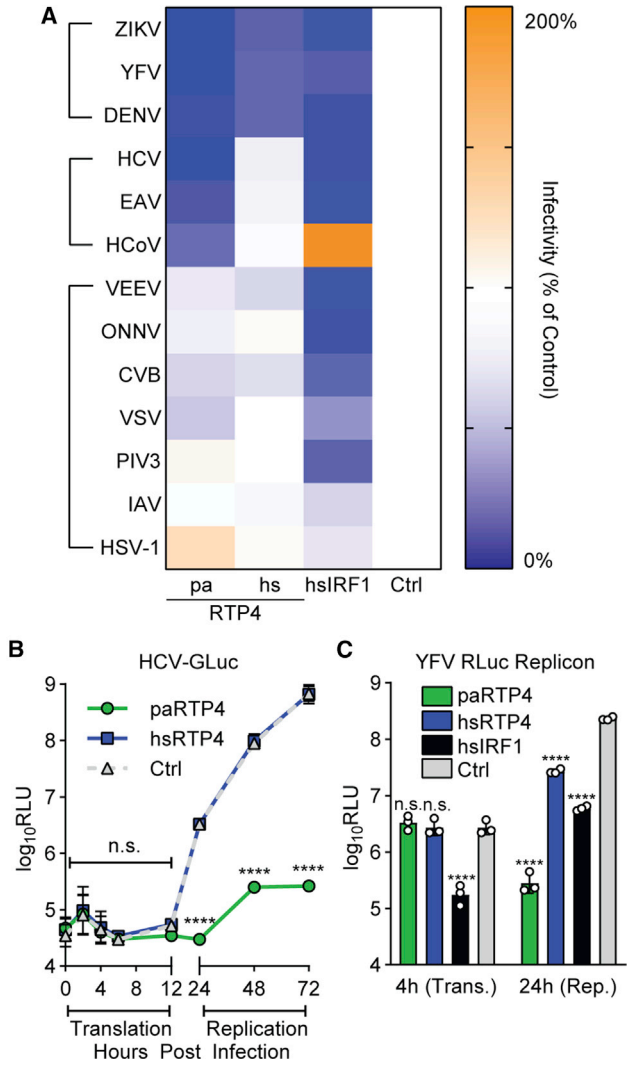


**Figure 2. RTP4 Restricts the Replication of Viruses that Replicate at the ER**

(A) Relative infectivity of cells expressing paRTP4, hsRTP4, hsIRF1, or an empty vector. Heatmap cells represent the mean of n = 3 biological replicates, normalized to control. For raw infectivity and experimental details, see Figure S2.

(B) HCV-GLuc infection of Huh7.5 cells expressing paRTP4, hsRTP4, or a vector control. Points indicate the mean ± SD relative light units (RLU) of n = 3 biological replicates. RM ANOVA on log-transformed data with Holm-Sidak test.

(C) Huh7.5 cells expressing paRTP4, hsRTP4, hsIRF1, or vector control were transfected with YFRluc2a replicon RNA. Bars represent mean ± SD RLU of n = 3 biological replicates. Two-way ANOVA on log-transformed data with Holm-Sidak test.

2019). Human RTP4, however, had only modest antiviral activity in our previous ISG screens (Schoggins et al., 2011) and was therefore not studied in detail.

RTP4 belongs to a family of proteins (RTP1s, RTP2, RTP3, and RTP4 in humans) that regulate the expression of cell-surface G-coupled protein receptors (Saito et al., 2004). Previous literature has implicated RTP4 as a regulator of opioid and taste receptors (Behrens et al., 2006; Décaillot et al., 2008), but its antiviral role has not been explored. RTP4 is the only known IFN-inducible member of the RTP protein family in humans and is conserved as an ISG across mammals (Shaw et al., 2017). We confirmed by qRT-PCR that *RTP4* is an ISG in black flying fox cells (Figure S1B). To validate our screen, we assessed the ability of ectopically expressed black flying fox RTP4, SHFL, and IFI6 to inhibit the flaviviruses ZIKV, DENV, and YFV and found that all three inhibited each virus tested (Figure 1C).

Humans and bats diverged roughly 96 million years ago (Kumar et al., 2017). At the amino acid level, human and black flying fox orthologs of SHFL, IFI6, and RTP4 share 95.1%, 67.7%, and 58.4% identity, respectively, suggesting that RTP4 may be a relatively divergent effector. We thus compared the ability of RTP4 from the black flying fox (*Pteropus alecto*, paRTP4) and humans (*Homo sapiens*, hsRTP4) to inhibit YFV when ectopically expressed in either human or black flying fox cells. In either species, paRTP4 exhibited greater antiviral activity than hsRTP4, suggesting that paRTP4 is functionally divergent and that this phenotype is not a result of the expression in a heterologous cellular background (Figures 1D–1F). Importantly, however, ectopically expressed paRTP4 expresses at much higher levels than hsRTP4 (Figure S1C) and therefore expression may contribute to differences in antiviral potency. To assess whether endogenous paRTP4 is antiviral, we used CRISPR-Cas9 to genetically ablate RTP4 in PaKi cells. Two clonal RTP4-knockout (KO) cell lines (Figures S1D) were challenged with YFV (Figure 1G). Loss of RTP4 led to enhanced infectivity relative to non-targeting control cell lines, albeit to a lesser degree than a STAT1 KO cell line (Figures S1E and S1F). We observed no difference in the binding of YFV to RTP4 KO cells relative to control cells (Figure S1G), suggesting that RTP4 ablation does not influence flavivirus receptor levels, as may have been expected given the role of RTP4 in chemosensory receptor trafficking (Décaillot et al., 2008).

## RTP4 Restricts the Replication of Viruses that Replicate at the ER

We next sought to determine the antiviral specificity of paRTP4 and hsRTP4. We compared the ability of ectopically expressed paRTP4 and hsRTP4 to restrict viruses from several families (Figures 2A and S2A). RTP4 orthologs exhibited strong (paRTP4) or modest (hsRTP4) antiviral activity against the flaviviruses (ZIKV, YFV, and DENV). paRTP4, but not hsRTP4, restricted the closely related *Flaviviridae* member, the hepacivirus hepatitis C virus (HCV), and to a lesser degree the nidoviruses equine arteritis virus (EAV), and human coronavirus OC43 (HCoV-OC43). Neither ortholog inhibited the picornavirus coxsackievirus B3 (CVB), the alphaviruses Venezuelan equine encephalitis virus (VEEV) and the o'nyong'nyong virus (ONNV), the rhabdovirus vesicular stomatitis virus (VSV), the paramyxovirus human parainfluenza virus type 3 (PIV3), the orthomyxovirus influenza A virus (IAV), or the herpes virus herpes simplex virus 1 (HSV-1). Of note, the viruses inhibited by both RTP4 orthologs are unified in their use of the host endoplasmic reticulum (ER) as a site for viral replication (Gillespie et al., 2010; Knoops et al., 2008). As a control, human IRF1 inhibited most viruses tested, as previously shown (Schoggins et al., 2014, 2011).

Since RTP4 potently inhibits flaviviruses, we next examined which step of the flavivirus life cycle it targets. We infected cells

expressing paRTP4, hsRTP4, or a vector control with a reporter HCV that expresses Gaussia luciferase (GLuc), which is secreted into culture supernatant when viral protein is translated (Figure 2B). This tool distinguishes early (entry and primary translation of incoming viral RNA) and late (genome replication) phases of infection. paRTP4 had no effect on GLuc production during primary translation but markedly reduced GLuc levels during viral replication. hsRTP4 did not reduce GLuc production at any time point, consistent with its lack of activity toward HCV observed when testing multiple viruses (Figure 2A). We next used a minimal, replication-competent, Renilla luciferase (RLuc)-expressing YFV RNA referred to as a "subgenomic replicon" to confirm that RTP4 targets the replication phase of viral infection. When transfected into cells, this naked viral RNA bypasses canonical viral entry routes and, similar to HCV-GLuc, distinguishes primary viral translation from genome amplification. Compared with human IRF1, which inhibits primary translation and replication (Schoggins et al., 2011), neither ortholog inhibited primary translation, and both inhibited replication, with paRTP4 exhibiting stronger antiviral activity than hsRTP4 (Figure 2C).

## The 3CXXC Zinc Finger Domain of Black Flying Fox RTP4 Is Necessary and Sufficient for Antiviral Activity

Previous literature has suggested that murine and human RTP4 are localized to the Golgi apparatus and the ER (Fujita et al., 2019). Since RTP4 inhibits ER-replicating viruses, we tested whether black flying fox RTP4 exhibits ER localization. Antibodies for bat RTP4 are not available, so we used CRISPR-mediated "gene-tagging" to fuse a hemagglutinin (HA) epitope tag to the N-terminus of endogenous RTP4 in PaKi cells (Figure S3A). Subcellular localization was assessed by immunofluorescence, using an anti-KDEL antibody and wheat germ agglutinin (WGA) as counterstains for the ER and the *trans*-Golgi network, respectively (Figure 3A). HA-tagged paRTP4 displayed an overlap with KDEL and only minimally overlapped with WGA signal, suggesting that endogenous paRTP4 is predominantly ER localized. Indeed, colocalization analysis revealed higher overlap between paRTP4 and KDEL than between either paRTP4 and WGA or KDEL and WGA (Figure S3B).

All RTP4 orthologs have three domains: an N-terminal 3CXXC zinc finger domain (ZFD), an intrinsically disordered variable region, and a transmembrane (TM) anchor (Figure 3B). We generated a 22 amino acid C-terminal truncation (paRTP4ΔTM) to determine whether the hydrophobic TM domain is required for localization and antiviral function. To confirm that paRTP4ΔTM was deficient for membrane association, we permeabilized cells expressing HA-tagged paRTP4 and paRTP4ΔTM with digitonin to release free cytosolic contents. Immunofluorescence microscopy and western blotting demonstrated that the membrane association of paRTP4ΔTM was lost as permeabilization promoted the release of paRTP4ΔTM (Figures 3C, S3C, and S3D). In the absence of digitonin treatment, paRTP4ΔTM significantly overlapped with KDEL (Figures 3C and S3C), suggesting that RTP4 localization does not solely depend upon its membrane anchor. Indeed, loss of membrane association did not abrogate the ability of paRTP4 to restrict YFV (Figure 3D). We next generated serial C-terminal truncations of paRTP4 (Figure 3E) and found that all truncations expressed to similar or greater levels as full-length paRTP4 (Figure 3F). None of the truncations, including an additional truncation (Δ246: C5), which deletes 57.5% of the protein, exhibited a substantial loss of antiviral activity (Figures 3G and S3E). These data suggest that the N-terminal 3CXXC ZFD of paRTP4 is sufficient for robust antiviral activity and that the disordered variable region is largely dispensable for inhibition of YFV, HCV, and HCoV-OC43.

We next mutated one cysteine in each conserved CXXC motif and a conserved histidine within the N-terminal ZFD (Figure 3H). C63A and C101A mutations resulted in decreased protein expression levels (Figure 3I), whereas proteins with H157A and C162A mutations expressed higher levels than wild-type paRTP4. All mutant proteins had a near-complete loss of antiviral activity in human cells (Figure 3J) suggesting that the CXXC motifs are critical for antiviral function. We next assessed the antiviral phenotype of a severe truncation (C4) and a well-expressed ZFD point mutant (C162A) in black flying fox cells to validate our findings in an autologous background. Truncated paRTP4 retained most of its antiviral activity, whereas perturbation of the ZFD completely disrupted its function (Figure 3K). Finally, to eliminate endogenous paRTP4 as a potential confounding factor, we reconstituted RTP4 KO cells with several paRTP4 constructs. Full-length and truncated (C5) paRTP4 were both antiviral, whereas paRTP4-H157A was not (Figure S3F). Together, these results suggest that the ZFD of paRTP4 is minimally required for antiviral function.

## Black Flying Fox RTP4 Binds Replicating Viral RNA and Suppresses Viral Genome Amplification

We next sought to gain insight into the molecular mechanism underlying the antiviral function of RTP4. Since paRTP4 nearly completely abrogates YFV replication, we used the related flavivirus WNV, which replicates at low levels in paRTP4-expressing cells when infected at high, but not low, multiplicity of infection (MOI) (Figures 4A and S4A). We first assessed whether RTP4 binds viral and/or host RNA because the 3CXXC ZFD of RTP4 is similar to that of the known RNA-binding proteins Zar1 and Zar2 (Charlesworth et al., 2012). Using cross-linking immunoprecipitation (CLIP) paired with qPCR, we found that RTP4 robustly binds sense and antisense viral RNA, as well as host RNAs, with no apparent bias toward any region of the viral genome (Figures 4B and S4B). The 3CXXC ZFD was sufficient for RNA binding, implicating it as the RNA-binding domain of RTP4 (Figure S4C). Similar results were found with YFV and endogenous paRTP4 in genomically tagged cells, suggesting that this interaction is not specific to WNV and that it occurs natively in black flying fox cells (Figure 4C).

Since RTP4 suppresses viral replication (Figures 2B and 2C), we investigated RNA-dependent processes upstream of viral assembly and egress. We used polysome profiling to determine whether paRTP4 affects the ribosome association of viral RNA, a critical step in translation. paRTP4 did not alter the association of WNV RNA with polysomes during infection (Figure 4D). However, the polysome association of *ACTB* mRNA differed between the control and paRTP4-expressing cells during infection (Figure 4D). This is consistent with decreased overall translation in highly infected vector control cells as indicated by a reduction in high-molecular-weight polysomes (Figure S4D). Together with our HCV reporter virus (Figure 2B) and YFV replicon data

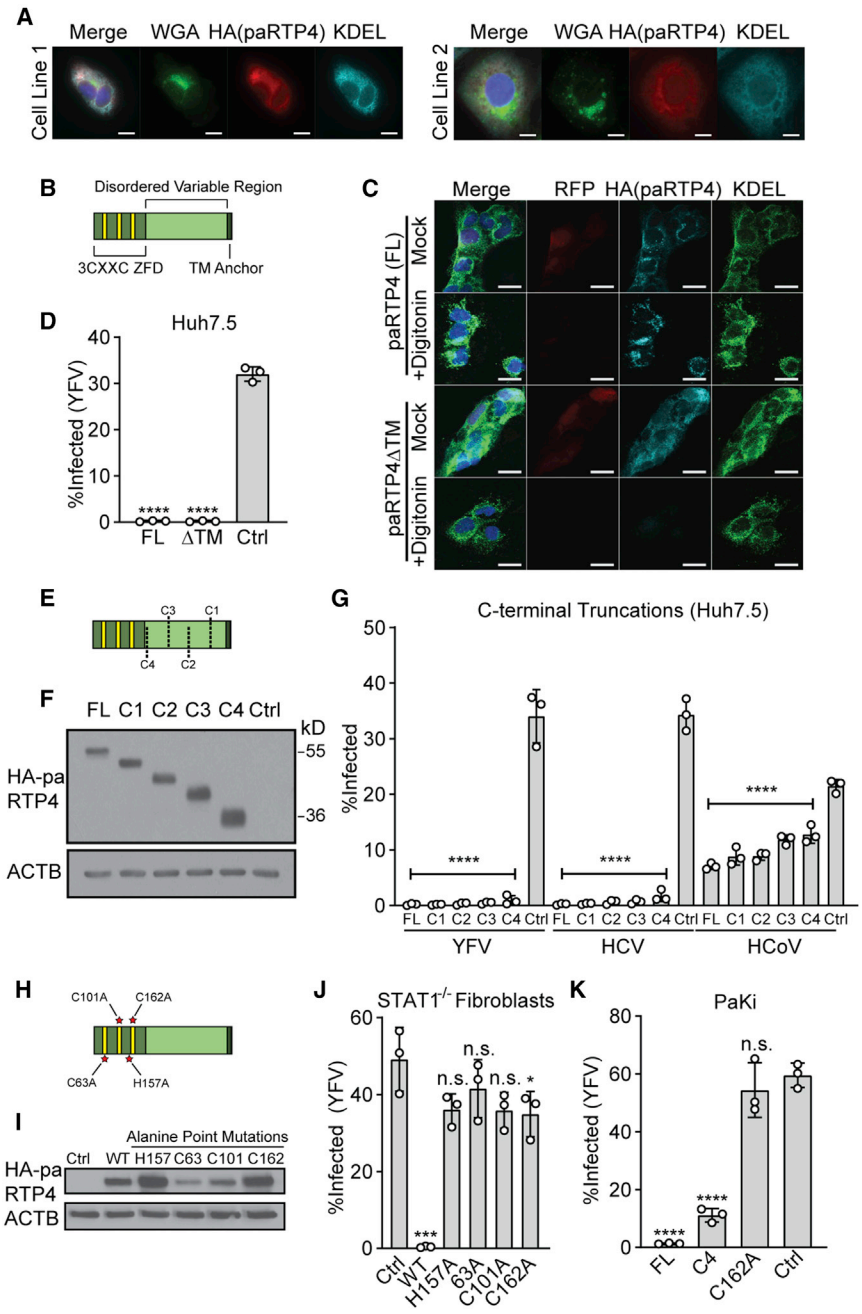


**Figure 3. The 3CXXC ZFD of Black Flying Fox RTP4 Is Necessary and Sufficient for Antiviral Activity**

(A) Endogenous RTP4 bearing a gene-edited HA epitope tag was detected in PaKi cells by tyramide signal amplification following treatment with 100 U/mL IFN for 8 h. Representative images of n = 3 biological replicates for two clonal cell lines. Linear adjustments were made to all channels separately. Scale bar represents 10 μm.

(B) Illustration depicting the 3CXXC ZFD, disordered variable region, and TM anchor of paRTP4.

(C) Huh7.5 cells expressing HA.paRTP4 or HA.paRTP4ΔTM were treated with digitonin prior to fixation. Cells were stained with antibodies against HA or KDEL. Co-expressed RFP serves as a control for untethered cytosolic contents, and KDEL serves as a control for membrane-bound proteins. Representative images of n = 3 biological replicates. Scale bar represents 20 μm.

(D) Huh7.5 cells expressing HA.paRTP4ΔTM, full-length HA.paRTP4, or a vector control were infected with YFV-Venus for 24 h. Bars represent mean ± SD of n = 3 biological replicates. One-way ANOVA with Dunnett's test.

(E) Illustration depicting serial C-terminal truncations of RTP4. C1:Δ56; C2:Δ106; C3:Δ156; C4:Δ206.

(F) Representative western blot (n = 3) of Huh7.5 cells expressing HA-tagged C-terminal truncations or full-length (FL) paRTP4.

(G) Huh7.5 cells expressing the indicated constructs were infected with YFV-Venus (24 h), HCV (48 h), or HCoV-OC43 (24 h). Bars represent mean ± SD of n = 3 biological replicates. One-way ANOVA with Dunnett's test.

(H) Illustration depicting ZFD-directed point mutations of RTP4.

(I) Western blot (n = 1) of STAT1$^{-/-}$ fibroblasts transduced with the indicated HA-tagged constructs.

(J) STAT1$^{-/-}$ fibroblasts transduced with the indicated constructs were infected with YFV-Venus. Bars represent mean ± SD of n = 3 biological replicates. One-way ANOVA with Dunnett's test.

(K) PaKi cells expressing the indicated constructs were infected with YFV-Venus. Bars represent mean ± SD of n = 3 biological replicates. One-way ANOVA with Dunnett's test.

(Figure 2C), this suggests that paRTP4 does not suppress the translation of viral protein.

Flavivirus RNA is amplified by two components of the viral replicase: NS5 (a multifunction enzyme that contains an RNA-dependent RNA polymerase) and NS3 (a multifunction enzyme that has helicase activity) (Lindenbach and Rice, 2003; Saeedi and Geiss, 2013). To determine whether paRTP4 inhibits genome amplification, we used flow cytometry and immunofluorescence to compare levels of NS5 and the intermediate replication product double-stranded RNA (dsRNA) in WNV-infected cells expressing either paRTP4 or a vector control. Surprisingly, while NS5 was present at similar levels, dsRNA was drastically reduced in paRTP4-expressing cells relative to control cells (Figures 4E and 4F). This confirms that paRTP4 does not block the production of viral protein but instead targets genome amplification. Since paRTP4 binds both sense and antisense viral RNA, we predicted that paRTP4 would associate with the site of viral replication. Indeed, a proximity ligation assay revealed apposition of paRTP5 with NS5 and paRTP4 with dsRNA, thereby localizing paRTP4 to active replication machinery (Figures 4G and S4E).

The coordinated activity of flavivirus NS3 and NS5 is required for viral replication. Since paRTP4 associates with replicating

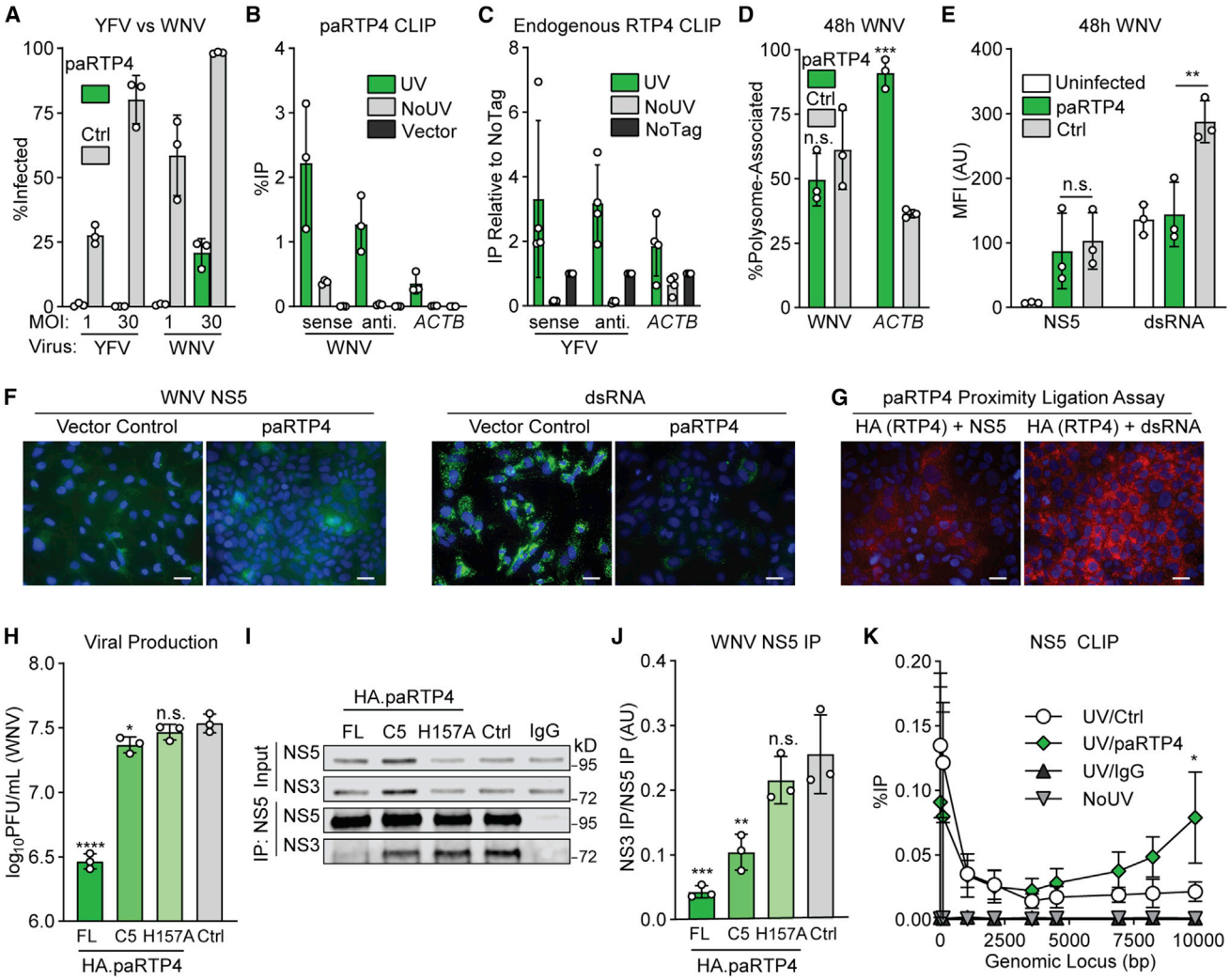


**Figure 4. Black Flying Fox RTP4 Binds Replicating Viral RNA and Suppresses Viral Genome Amplification**

(A) Huh7.5 cells expressing HA.paRTP4 or a vector control were infected with WNV or YFV-17D (MOI of 1 or 30) and harvested at 24 h. Bars represent mean ± SD of n = 3 biological replicates. See Figure S4A.

(B) Huh7.5 cells expressing HA.paRTP4 or a vector control were infected with WNV (MOI of 30) for 48 h. CLIP-qPCR identified RNA bound by RTP4. UV, UV-crosslinked HA.paRTP4 cells; NoUV, non-crosslinked HA.paRTP4 cells; Vector, UV-crosslinked vector control cells. Bars represent mean ± SD of n = 3 biological replicates. See Figures S4B and S4C.

(C) PaKi cells were infected with YFV-17D (MOI of 5) for 48 h. CLIP-qPCR identified RNA bound by HA.paRTP4. UV, crosslinked endogenously tagged cells; NoUV, non-crosslinked endogenously tagged cells; NoTag, crosslinked wild-type cells. Bars represent mean ± SD of n = 4 biological replicates.

(D) Polysome association of WNV vRNA and *ACTB* in Huh7.5 cells expressing HA.paRTP4 or a vector control infected with WNV (MOI of 30) for 48 h. Bars represent mean ± SD of n = 3 biological replicates. Two-way ANOVA with Holm-Sidak test. See Figure S4D.

(E) Huh7.5 cells expressing HA.paRTP4 or FLuc as a negative control were infected with WNV (MOI of 30) for 48 h. NS5 and dsRNA levels were quantified by flow cytometry. Bars represent mean ± SD of n = 3 biological replicates. Two-way ANOVA with Holm-Sidak test.

(F) Huh7.5 cells expressing HA.paRTP4 or a vector control were infected with WNV (MOI of 30) for 48 h. NS5 and dsRNA levels were visualized by immunofluorescence microscopy. Representative image of n = 3 biological replicates. Scale bar represents 30 μm.

(G) Huh7.5 cells expressing HA.paRTP4 were infected with WNV (MOI of 30) for 48 h. A proximity ligation assay was performed for HA and either NS5 or dsRNA. Representative image of n = 2 biological replicates. Scale bar represents 30 μm. For PLA controls, see Figure S4E.

(H) Huh7.5 cells expressing the indicated paRTP4 constructs were infected with WNV (MOI of 30) for 48 h. Quantification by plaque assay. Bars represent mean ± SD of n = 3 biological replicates. One-way ANOVA with Dunnett's test performed on log-transformed data.

(I) Huh7.5 cells expressing the indicated paRTP4 constructs were infected with WNV (MOI of 30) for 48 h WNV NS5 was immunoprecipitated, and quantitative western blotting was performed using a Li-COR imager. Representative blot of n = 3 biological replicates.

(J) Quantification of (I) showing the co-immunoprecipitation of NS3 by NS5, normalized to NS5 pull-down efficiency. Bars represent mean ± SD of n = 3 biological replicates. One-way ANOVA with Dunnett's test.

(K) Huh7.5 cells expressing HA.paRTP4 or a vector control were infected with WNV (MOI of 30) for 48 h. CLIP-qPCR with limited nuclease digestion identified the binding profile of NS5 on viral genomic RNA. UV/Ctrl, crosslinked vector control cells, IP NS5; UV/RTP4, crosslinked paRTP4-expressing cells, IP NS5; UV/IgG, crosslinked control cells, IP IgG; NoUV, non-crosslinked vector control cells, IP NS5. Bars represent mean ± SD of n = 3 biological replicates. Two-way ANOVA with Holm-Sidak test.

**Table 1. PAML Analysis of Mammalian *RTP4***

| Clade | No. of Sequences | *P* (M7 versus M8) | *P* (M8a versus M8) | # Positively Selected Sites | dN/dS—Full | dN/dS—ZFD | dN/dS—CTD |
|---|---|---|---|---|---|---|---|
| Bats | 9 | 6.19E-12 | 1.36E-12 | 16 | 1.11435 | 0.54532 | 1.69034 |
| Ungulates | 9 | 0.0007 | 0.0002 | 2 | 0.88649 | 0.57696 | 1.15441 |
| Carnivores | 11 | 0.1490 | 0.0765 | 3 | 0.66288 | 0.27508 | 1.21071 |
| Rodents | 10 | 0.0119 | 0.0041 | 11 | 0.66831 | 0.54678 | 1.03903 |
| Primates | 11 | 0.0167 | 0.0043 | 1 | 0.69046 | 0.52927 | 1.30167 |

Positively selected sites are those with an M8 BEB >95%. Both M7 versus M8 and M8a versus M8 tests compare site models, which allow positive selection (M8) and those that do not (M7, M8a). For related data, see Figure S5 and Data S2.

viral RNA, we hypothesized that paRTP4-mediated restriction of genome amplification may alter interactions between NS3 and NS5. Co-immunoprecipitation and quantitative western blotting revealed that the association of WNV NS5 and NS3 is roughly 6-fold lower in paRTP4-expressing cells relative to control cells (Figures 4I and 4J). Furthermore, WNV NS3-NS5 association correlates (R-squared 0.859) with viral production in the presence of paRTP4 constructs that exhibit reduced antiviral activity (C5, H157A) relative to full-length paRTP4 when infected at a high MOI (Figures 4H, S4F, and S4G). We additionally used CLIP with limited nuclease digestion and found that the binding profile of NS5 across the WNV genome is skewed in paRTP4-expressing cells relative to control cells (Figure 4K). This skewed binding is consistent with a model where RTP4, perhaps by binding replicating viral RNA, perturbs events that occur during genome amplification, likely resulting in the dramatic reduction in dsRNA production as depicted in Figures 4E and 4F.

## RTP4 Is a Species-Specific Mammalian Restriction Factor

Although hsRTP4 and paRTP4 express at different levels (Figure S1C), we suspected that expression alone could not explain drastic differences in antiviral potential such as the ability of paRTP4 to inhibit HCV while hsRTP4 does not (Figures 2A and 2B). We noted that hsRTP4 and paRTP4 differ substantially in length (246 and 428 amino acids, respectively), and a comparison of protein lengths in therian (live-bearing) mammals revealed that while other antiviral effectors exhibit a unimodal distribution of protein lengths, RTP4 lengths are trimodal, ranging from just under 200 to over 600 residues (Figure S5A). This suggested that neither hsRTP4 nor paRTP4 is uniquely representative of mammalian RTP4s, and we thus expanded our studies to include RTP4 orthologs from multiple mammalian lineages.

Antiviral effectors often exhibit signatures of pervasive positive selection, as they are hotspots in the "molecular arms race" between viruses and their hosts (Daugherty and Malik, 2012). Using phylogenetic analysis by maximum likelihood (PAML) (Yang, 1993), we found that RTP4 displays a signature of rapid evolution in several mammalian lineages (bats, ungulates, carnivores, rodents, and primates) (Table 1; Figure S5B). Notably, bats comprise the only lineage that displays a gene-wide dN/dS (the ratio of non-synonymous over synonymous codon changes at a given site) of greater than 1, indicative of robust positive selection. All lineages display a dN/dS > 1 for their C-terminal variable region, and no lineage has a dN/dS > 1 for its ZFD alone. Furthermore, a free-ratio analysis of bat RTP4 in PAML produced dN/dS ratios > 1 on several branches in both bat suborders (Yinpterochiroptera and Yangochiroptera), indicative of widespread episodic positive selection (Figure S5C). These data are consistent with a model in which RTP4 and the viruses that it inhibits are locked in a classic "Red Queen conflict" (Van Valen, 1973), wherein RTP4 in diverse species has adapted over evolutionary time to the selective pressures imposed by constantly evolving viruses.

To explore functional consequences of this genetic conflict, we compared the ability of RTP4 orthologs from three bat species (two megabats, the black flying fox and the Egyptian fruit bat; one microbat, the Mexican free-tailed bat), two ungulates (cow and pig), one carnivore (dog), two primates (human and rhesus macaque), and one rodent (house mouse) to restrict a panel of flaviviruses (DENV, ZIKV, WNV, YFV, and Entebbe bat virus [ENTV]), the hepacivirus HCV, and the nidoviruses EAV and HCoV-OC43. We found that different RTP4 orthologs exhibit striking species- and lineage-specific properties (Figure 5A). Although protein expression levels varied among the orthologs, a hierarchical clustering approach (Baker, 1974) suggests that phylogeny is closely correlated with the antiviral phenotype (Baker's Gamma Index: phenotype/expression 0.03; phenotype/phylogeny 0.79; phylogeny/expression −0.17) (Figures S6A and S6B). There are, however, instances where expression levels trend with differences in antiviral potency. Among bats, black flying fox RTP4 was expressed at the highest levels and most potently restricted all viruses. Among ungulates, cow RTP4 was expressed at roughly twice the levels of pig RTP4 and was typically more antiviral. However, there are instances where the expression does not predict potency. For example, mouse RTP4, despite expressing at roughly the same level as the broadly inhibitory cow RTP4, is the weakest effector against most viruses, only potently restricting HCV. To further address the relationship between protein expression and viral inhibition, we used a doxycycline-inducible HA-tagged paRTP4 construct to titrate paRTP4 expression levels prior to YFV infection and found that paRTP4 inhibited YFV in a dose-dependent manner (Figure S6C).

If evolutionary pressure has driven the specialization of different RTP4 orthologs, we would predict that (1) an ancestral RTP4 would be antiviral, and (2) it would perhaps exhibit less specialization than the evolutionarily honed mammalian RTP4 orthologs that exist in nature. We used maximum-likelihood modeling to infer an ancestral RTP4 sequence (asrRTP4) based on data from 35 mammalian genomes representative of 96 million years of evolution (Data S2). We synthesized asrRTP4

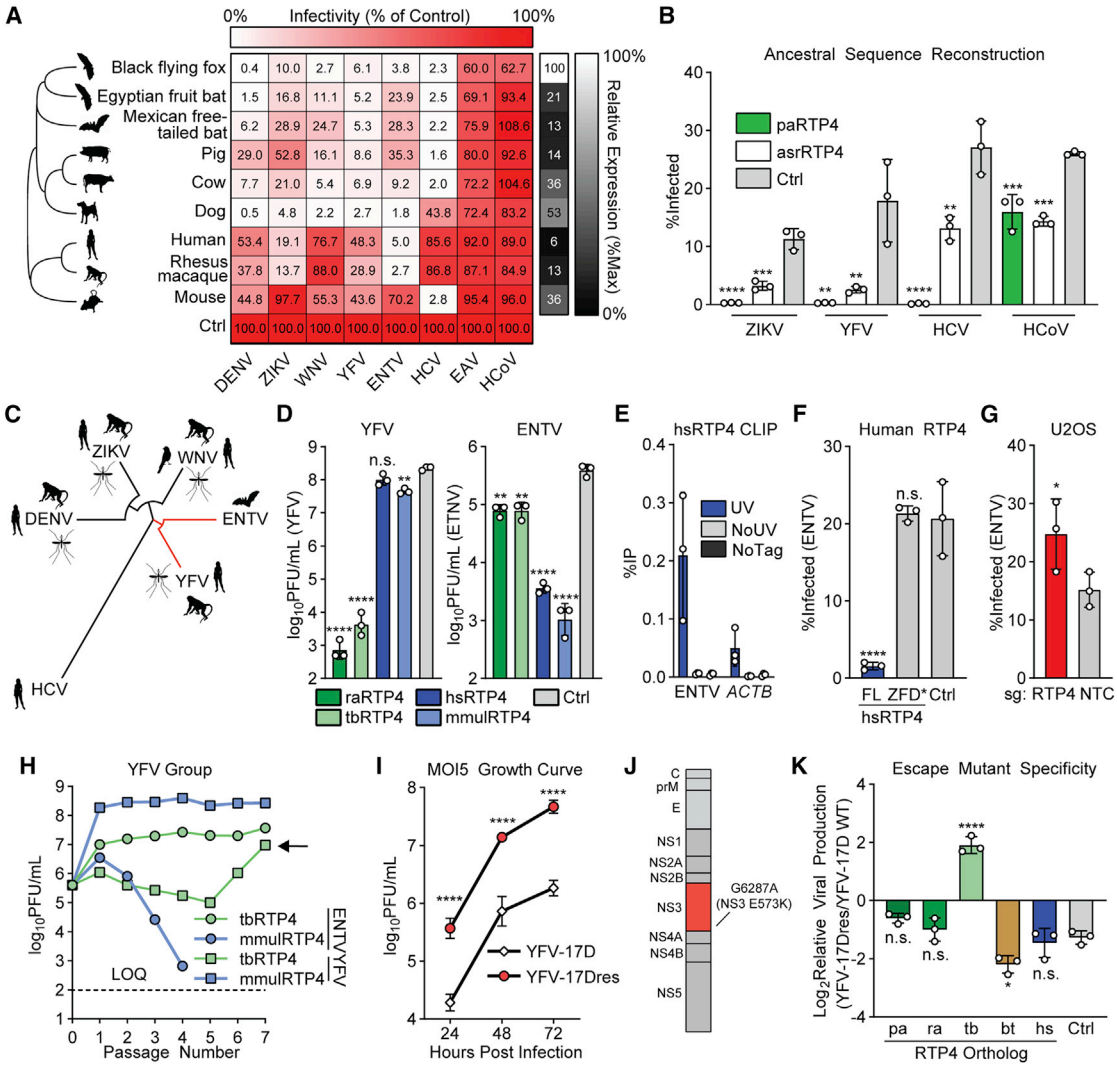


**Figure 5. RTP4 Is a Species-Specific Mammalian Restriction Factor**

(A) Huh7.5 cells expressing HA-tagged RTP4 orthologs or a vector control were infected with the indicated viruses. Large heatmap: cells represent the mean infectivity of n = 3 biological replicates, normalized to within-replicate control. Small heatmap: cells represent the mean protein expression of n = 3 biological replicates, relative to ACTB and normalized to within-replicate maximum expression. For raw infectivity data, see Table S2.

(B) Huh7.5 cells expressing paRTP4, asrRTP4, or a control were infected with the indicated viruses. Bars represent mean ± SD of n = 3 biological replicates. One-way ANOVA with Dunnett's test.

(C) Maximum-likelihood phylogenetic tree for polyprotein of flaviviruses screened in (A). Common amplifying hosts are indicated by silhouettes.

(D) Huh7.5 cells expressing the indicated constructs were infected with YFV-17D and ENTV (MOI of 0.05) for 24 h (ENTV) or 48 h (YFV). Quantification by plaque assay. Bars represent mean ± SD of n = 3 biological replicates. One-way ANOVA with Dunnett's test performed on log-transformed data.

(E) Huh7.5 cells expressing either HA-tagged hsRTP4 or untagged hsRTP4 as a control were infected with ENTV (MOI of 5) for 24 h. CLIP-qPCR identified RNA bound by RTP4. UV, UV-crosslinked HA.hsRTP4 cells; NoUV, non-crosslinked HA.hsRTP4 cells; NoTag, UV-crosslinked hsRTP4 cells. Bars represent mean ± SD of n = 3 biological replicates.

(F) Huh7.5 cells expressing the indicated hsRTP4 constructs were infected with ENTV at an MOI of 0.5 for 16 h. Bars represent mean ± SD of n = 3 biological replicates. One-way ANOVA with Dunnett's test.

(G) CRISPR-targeted U2OS cells were infected with ENTV (MOI of 2.5) for 24 h. Bars represent mean ± SD of n = 3 biological replicates. Paired two-tailed t test.

(H) Cells expressing rhesus macaque (mmul) or Mexican free-tailed bat (tb) RTP4 were infected with ENTV or YFV-17D (MOI of 5). Supernatant was collected at 24 h (ENTV) or 48 h (YFV) and transferred to naive cells for seven passages. Quantification by plaque assay. Points represent n = 1 plaque assay.

(I) Huh7.5 cells expressing tbRTP4 were infected with YFV-17D or YFV-17Dres$_p$ (MOI of 5) for 72 h. Quantification by plaque assay. Points indicate the mean ± SD of n = 3 biological replicates. Two-way ANOVA on log-transformed data with Holm-Sidak test.

(J) Illustration representing the YFV polyprotein. NS3 point mutation is indicated.

(K) Huh7.5 cells expressing the indicated RTP4 constructs or a vector control were infected with YFV-17D or YFV-17Dres$_c$ (MOI of 5) for 24 h. Quantification by plaque assay. The ratio of viral production from wild-type YFV-17D and YFV-17Dres$_c$ is shown. Bars represent mean ± SD of n = 3 biological replicates. One-way ANOVA with Dunnett's test. See Figures S6J and S6K.

and assessed its ability to inhibit infection by YFV, ZIKV, HCV, and HCoV-OC43. We found that asrRTP4, which expresses at roughly 65% the level of paRTP4 (Figure S6D), inhibited each virus, albeit with limited potency relative to paRTP4 for ZIKV, YFV, and HCV (Figure 5B). As with less-inhibitory orthologs, relative expression levels may explain some of its decreased potency, though its weak phenotype toward HCV and relative strength against HCoV are unique among RTP4 proteins. This supports a model in which RTP4 has been selected for enhanced activity toward certain, but not all, viruses in different mammalian lineages, and is consistent with research on other antiviral effectors such as the plant Rx protein and mammalian MX1, which exhibit a trade-off between potency and specificity (Farnham and Baulcombe, 2006; Colón-Thillet et al., 2019).

We noted that RTP4 from two bats, the Egyptian fruit bat (raRTP4) and the Mexican free-tailed bat (tbRTP4), and two primates, humans and the rhesus macaque (mmulRTP4), exhibited opposite antiviral phenotypes during ENTV and YFV infection (Figure 5A). ENTV is a bat-specific, non-vectored flavivirus that belongs to the YFV group, and is the closest relative to YFV within our screen (Figure 5C) (Simmonds et al., 2017). We validated by plaque assay that ectopically expressed mmulRTP4 and hsRTP4 potently restrict ENTV, but not YFV, whereas tbRTP4 and raRTP4 potently restrict YFV, but not ENTV (Figure 5D).

ENTV is the only virus that is potently inhibited by hsRTP4 among all viruses screened in the present work (Figures 2A and 5A) and our previous publications (Schoggins et al., 2014, 2011). To assess the significance of RTP4 as a human antiviral effector, we explored whether our mechanistic findings for paRTP4 could be recapitulated with hsRTP4 in the context of ENTV. CLIP-qPCR showed that hsRTP4 binds ENTV RNA during infection (Figure 5E), and a ZFD-targeted point mutation disrupts its antiviral function (Figures 5F and S6E). Importantly, we found that CRISPR-based silencing of RTP4 in human U2OS osteosarcoma cells resulted in increased ENTV infection relative to non-targeting control cells, suggesting that endogenous hsRTP4 is antiviral (Figure 5G). This result is similar to the findings obtained in gene silencing studies of broadly inhibitory black flying fox (Figure 1G) and pig (Figure S6F) RTP4 orthologs in the context of YFV infection. These data suggest that human RTP4 is not a "weak" RTP4 ortholog—instead, it is best adapted to inhibit certain viruses, such as ENTV, and is poorly adapted to inhibit others, such as YFV.

The error-prone nature of RNA virus replication often allows the emergence of viral variants that can overcome selective pressure, such as that imposed by a restriction factor (Domingo et al., 2012). We observed that some viruses resisted inhibition by certain RTP4 orthologs (Figure 5A), suggesting that adaptive evolution may have enabled escape from RTP4-mediated restriction in a species-specific manner. To model this experimentally, we serially passaged YFV and ENTV in cells expressing tbRTP4 or mmulRTP4 to determine if either virus could overcome the antiviral effects of an RTP4 ortholog that inhibits it. After six passages, we obtained a YFV escape mutant (YFV-17D$Dres_p$) that was able to replicate in the presence of tbRTP4 (Figure 5H). We did not obtain an mmulRTP4 ENTV escape mutant (Figure 5H) or paRTP4 WNV escape mutant (Figure S6G). YFV-17D$Dres_p$ exhibits roughly 10-fold enhanced replication in tbRTP4-expressing cells as compared to YFV-17D (Figure 5I). Sequencing of clonal escape mutants identified a single point mutation (G6287A) that results in a missense E573K mutation in NS3 (Figures 5J and S6H; Table S3). An engineered virus (YFV-17D$Dres_c$) containing this mutation phenocopied YFV-17D$Dres_p$ (Figure S6I). We compared the replicative capacity of YFV-17D$Dres_c$ in the presence of RTP4 from other bats (black flying fox and Egyptian fruit bat), cow, or humans to determine (1) if this escape was specific to freetail bat RTP4, and (2) if the mutation attenuates the virus. Indeed, we found that although this mutation confers enhanced replication in the presence of tbRTP4, YFV-17D$Dres_c$ was attenuated relative to wild-type virus in cells expressing other mammalian RTP4s (Figures 5K, S6J, and S6K). This complements our phylogenetic analysis (Table 1) and the specificity observed in our ortholog screen (Figure 5A), providing evidence that RTP4 may be involved in a classic Red Queen conflict with flaviviruses, in which diversification of both hosts and viruses has yielded a complex pattern of antiviral specificity of mammalian RTP4 orthologs.

## DISCUSSION

In the present study, we identify black flying fox (*Pteropus alecto*) RTP4 as a potent anti-flavivirus effector that binds viral RNA and restricts viral genome amplification. We find that RTP4-mediated restriction is associated with alterations in the flavivirus replicase (Figures 4I–4K) and that a virus can escape RTP4-mediated restriction through a mutation in NS3, a component of its replicase (Figures 5H–5K). Uncovering the precise molecular mechanism of RTP4-mediated inhibition may provide insight into novel therapeutic targets, as well as further our understanding of flavivirus genome replication. Our observation that black flying fox and human RTP4 exhibit differential phenotypes (Figure 2) led us to test the inhibitory potential of RTP4 orthologs from several species, and we uncovered an intricate pattern of antiviral specificity across Mammalia (Figure 5A). Our study is only representative of the approximately 70 known flaviviruses, half of which are considered potential human pathogens (Simmonds et al., 2017). Screening more diverse mammalian RTP4s against other flaviviruses may reveal additional layers of specificity underlying this virus-host conflict.

Often, studies of immune effectors with species-specific antiviral activity have focused on the careful comparison of orthologs from closely related species to identify genetic signatures of recurrent, or pervasive, positive selection. Pervasive positive selection is a hallmark of the molecular application of Leigh Van Valen's "Red Queen hypothesis," which posits that co-existing organisms must continually adapt to pressures imposed by one another in order to survive (Van Valen, 1973). Notable examples of host-virus molecular arms races include TRIM5$\alpha$, where a positively selected patch of residues underlies differences in antiretroviral potency of rhesus and human orthologs, (Sawyer et al., 2005) and MX1, where a single positively selected residue confers the ability of human MX1 to inhibit certain orthomyxoviruses (Mitchell et al., 2012). Our functional comparative study of representative RTP4 orthologs from diverse mammalian clades complements such approaches and highlights the value of looking beyond closely related species when investigating host-virus conflicts. Indeed, although there is evidence of positive selection

in RTP4 in multiple lineages, we do not find positively selected patches of residues that are common among lineages (Table 1; Figure S5B). This could suggest that the Red Queen conflicts between RTP4 orthologs and the viruses that they inhibit have led to unique innovations both in viruses and their mammalian hosts. Importantly, this model is supported experimentally by the emergence of a viral variant that escapes inhibition by one RTP4 ortholog but not by others (Figure 5K). We suspect that evolutionary pressure imposed by inhibitory RTP4s may have driven viral adaptation, with a possible fitness cost being the impairment of replication due to a mutation in NS3. Conversely, over long evolutionary timescales, mammals may have incurred flavivirus-driven fitness costs that drove complex RTP4 adaptations, including single amino acid changes and modifications to the intrinsically disordered C-terminal domain. Notably, a recent study (He et al., 2020) has found that RTP4 in humans and mice is a negative regulator of IFN signaling. It is tempting to speculate that RTP4 may have evolved unique regulatory functions across Mammalia in addition to its pathogen-driven evolution as an antiviral effector.

## STAR★METHODS

Detailed methods are provided in the online version of this paper and include the following:

- KEY RESOURCES TABLE
- RESOURCE AVAILABILITY
  - Lead Contact
  - Materials Availability
  - Data and Code Availability
- EXPERIMENTAL MODEL AND SUBJECT DETAILS
  - Cell Culture
  - Viruses
- METHOD DETAILS
  - Lentiviral Pseudoparticle Production and Transductions
  - AAV Production
  - CRISPR Editing
  - Transfection of PaKi Cells
  - Viral Infections
  - Plaque Assays
  - Crystal Violet Stains
  - Intracellular Antibody Staining for Flow Cytometry
  - Flow Cytometry
  - Digitonin Membrane Association Assays
  - CLIP-qPCR
  - Polysome Profiling
  - Quantitative RT-PCR
  - Immunofluorescence
  - Tyramide Signal Amplification
  - Proximity Ligation Assay
  - Immunoprecipitations
  - cDNA Library Construction
  - Screen for Antiviral bat cDNAs
  - Plasmids and Cloning
  - *In Vitro* Transcription of Viral and Replicon RNA
  - Electroporation of Viral RNA
  - Western Blotting
  - Replicon Assay
  - HCV-GLuc Assay
  - Viral Cold Bind-qPCR Assay
  - Doxycycline Induction for Viral Infections
  - Serial Passaging and Viral Sequencing
  - Phylogenetic Analysis
  - Ancestral Sequence Reconstruction
  - Clustering and Correlation Analysis of Phylogenetic, Expression, and Infectivity Data
  - Colocalization Analysis
  - RNA Sequencing & Analysis
  - ISG Length Comparison
- QUANTIFICATION AND STATISTICAL ANALYSIS

## SUPPLEMENTAL INFORMATION

Supplemental Information can be found online at https://doi.org/10.1016/j.chom.2020.09.014.

## ACKNOWLEDGMENTS

We thank Lin-Fa Wang for providing PaKi cells; Susan J. Wong for providing WNV NS3 and NS5 antibodies; Nicholas Conrad, Dustin Hancks, and Maikke Ohlson for critical manuscript feedback; and Julio Ruiz, Anna Scarborough, and Nicholas Conrad for helpful discussions. We acknowledge the UT Southwestern (UTSW) Bioinformatics Lab for their assistance. This study was in part supported by grants to J.W.S. (NIH AI117922, UTSW High Impact/High Risk Grant Program, UTSW Endowed Scholars Program, the Rita Allen Foundation, The Welch Foundation [I-2013-20190330], and an Investigators in the pathogenesis of Infectious Disease Award from the Burroughs Wellcome Fund). I.N.B. was supported by the NSF GRFP (grant no. 2016217834) and NIH T32 training grant AI005284. K.B.M. was supported by the NIH T32 training grant AI005284. E.X. was supported by the Amgen Foundation through the Amgen Scholars program. Any opinion, findings, and conclusions or recommendations expressed in this material are those of the authors(s) and do not necessarily reflect the views of funding agencies.

## AUTHOR CONTRIBUTIONS

Conceptualization, I.N.B. and J.W.S.; Investigation, I.N.B., E.X., and K.B.M.; Resources, I.N.B., E.X., P.C.D.L.C.-R., J.L.E., B.M., and K.B.M.; Writing, I.N.B. and J.W.S.; Visualization, I.N.B.; Funding Acquisition, I.N.B. and J.W.S.

## DECLARATION OF INTERESTS

The authors declare no competing interests.

Received: June 12, 2020
Revised: August 19, 2020
Accepted: September 15, 2020
Published: October 27, 2020

## REFERENCES

Ahn, M., Anderson, D.E., Zhang, Q., Tan, C.W., Lim, B.L., Luko, K., Wen, M., Chia, W.N., Mani, S., Wang, L.C., et al. (2019). Dampened NLRP3-mediated inflammation in bats and implications for a special viral reservoir host. Nat. Microbiol. *4*, 789–799.

Ashkenazy, H., Penn, O., Doron-Faigenboim, A., Cohen, O., Cannarozzi, G., Zomer, O., and Pupko, T. (2012). FastML: a web server for probabilistic reconstruction of ancestral sequences. Nucleic Acids Res. *40*, W580–W584.

Baker, F.B. (1974). Stability of two hierarchical grouping techniques case I: sensitivity to data errors. J. Am. Stat. Assoc. *69*, 440–445.

Balinsky, C.A., Schmeisser, H., Wells, A.I., Ganesan, S., Jin, T., Singh, K., and Zoon, K.C. (2017). IRAV (FLJ11286), an interferon-stimulated gene with

antiviral activity against dengue virus, interacts with MOV10. J. Virol. *91*, 1606–1616.

Banerjee, A., Zhang, X., Yip, A., Schulz, K.S., Irving, A.T., Bowdish, D., Golding, B., Wang, L.F., and Mossman, K. (2020). Positive selection of a serine residue in bat IRF3 confers enhanced antiviral protection. iScience *23*, 100958.

Behrens, M., Bartelt, J., Reichling, C., Winnig, M., Kuhn, C., and Meyerhof, W. (2006). Members of RTP and REEP gene families influence functional bitter taste receptor expression. J. Biol. Chem. *281*, 20650–20659.

Benfield, C.T., MacKenzie, F., Ritzefeld, M., Mazzon, M., Weston, S., Tate, E.W., Teo, B.H., Smith, S.E., Kellam, P., Holmes, E.C., and Marsh, M. (2020). Bat IFITM3 restriction depends on S-palmitoylation and a polymorphic site within the CD225 domain. Life Sci. Alliance *3*.

Calisher, C.H., Childs, J.E., Field, H.E., Holmes, K.V., and Schountz, T. (2006). Bats: important reservoir hosts of emerging viruses. Clin. Microbiol. Rev. *19*, 531–545.

Castresana, J. (2000). Selection of conserved blocks from multiple alignments for their use in phylogenetic analysis. Mol. Biol. Evol. *17*, 540–552.

Charlesworth, A., Yamamoto, T.M., Cook, J.M., Silva, K.D., Kotter, C.V., Carter, G.S., Holt, J.W., Lavender, H.F., MacNicol, A.M., Ying Wang, Y., and Wilczynska, A. (2012). Xenopus laevis zygote arrest 2 (zar2) encodes a zinc finger RNA-binding protein that binds to the translational control sequence in the maternal Wee1 mRNA and regulates translation. Dev. Biol. *369*, 177–190.

Colón-Thillet, R., Hsieh, E., Graf, L., McLaughlin, R.N., Jr., Young, J.M., Kochs, G., Emerman, M., and Malik, H.S. (2019). Combinatorial mutagenesis of rapidly evolving residues yields super-restrictor antiviral proteins. PLoS Biol. *17*, e3000181.

Conrad, N.K. (2008). Chapter 15. Co-immunoprecipitation techniques for assessing RNA-protein interactions in vivo. Methods Enzymol. *449*, 317–342.

Crameri, G., Todd, S., Grimley, S., McEachern, J.A., Marsh, G.A., Smith, C., Tachedjian, M., De Jong, C., Virtue, E.R., Yu, M., et al. (2009). Establishment, immortalisation and characterisation of pteropid bat cell lines. PLoS One *4*, e8266.

Daugherty, M.D., and Malik, H.S. (2012). Rules of engagement: molecular insights from host-virus arms races. Annu. Rev. Genet. *46*, 677–700.

De La Cruz-Rivera, P.C., Kanchwala, M., Liang, H., Kumar, A., Wang, L.F., Xing, C., and Schoggins, J.W. (2018). The IFN response in bats displays distinctive IFN-stimulated gene expression kinetics with atypical RNaseL induction. J. Immunol. *200*, 209–217.

Décaillot, F.M., Rozenfeld, R., Gupta, A., and Devi, L.A. (2008). Cell surface targeting of mu-delta opioid receptor heterodimers by RTP4. Proc. Natl. Acad. Sci. USA *105*, 16045–16050.

Dobin, A., Davis, C.A., Schlesinger, F., Drenkow, J., Zaleski, C., Jha, S., Batut, P., Chaisson, M., and Gingeras, T.R. (2013). STAR: ultrafast universal RNA-seq aligner. Bioinformatics *29*, 15–21.

Domingo, E., Sheldon, J., and Perales, C. (2012). Viral quasispecies evolution. Microbiol. Mol. Biol. Rev. *76*, 159–216.

Dukhovny, A., Lamkiewicz, K., Chen, Q., Fricke, M., Jabrane-Ferrat, N., Marz, M., Jung, J.U., and Sklan, E.H. (2019). A CRISPR activation screen identifies genes that protect against Zika virus infection. J. Virol. *93*, e00211–e00219.

Farnham, G., and Baulcombe, D.C. (2006). Artificial evolution extends the spectrum of viruses that are targeted by a disease-resistance gene from potato. Proc. Natl. Acad. Sci. USA *103*, 18828–18833.

Fuchs, J., Hölzer, M., Schilling, M., Patzina, C., Schoen, A., Hoenen, T., Zimmer, G., Marz, M., Weber, F., Müller, M.A., and Kochs, G. (2017). Evolution and antiviral specificities of interferon-induced Mx proteins of bats against Ebola, influenza, and other RNA viruses. J. Virol. *91*, e00361-17.

Fujita, W., Yokote, M., Gomes, I., Gupta, A., Ueda, H., and Devi, L.A. (2019). Regulation of an opioid receptor chaperone protein, RTP4, by morphine. Mol. Pharmacol. *95*, 11–19.

Galili, T. (2015). dendextend: an R package for visualizing, adjusting and comparing trees of hierarchical clustering. Bioinformatics *31*, 3718–3720.

Gillespie, L.K., Hoenen, A., Morgan, G., and Mackenzie, J.M. (2010). The endoplasmic reticulum provides the membrane platform for biogenesis of the Flavivirus replication complex. J. Virol. *84*, 10438–10447.

Glez-Peña, D., Gómez-Blanco, D., Reboiro-Jato, M., Fdez-Riverola, F., and Posada, D. (2010). ALTER: program-oriented conversion of DNA and protein alignments. Nucleic Acids Res. *38*, W14–W18.

Halpin, K., Young, P.L., Field, H.E., and Mackenzie, J.S. (2000). Isolation of Hendra virus from pteropid bats: a natural reservoir of Hendra virus. J. Gen. Virol. *81*, 1927–1932.

Hanners, N.W., Eitson, J.L., Usui, N., Richardson, R.B., Wexler, E.M., Konopka, G., and Schoggins, J.W. (2016). Western Zika virus in human fetal neural progenitors persists long term with partial cytopathic and limited immunogenic effects. Cell Rep. *15*, 2315–2322.

Hawkins, J.A., Kaczmarek, M.E., Müller, M.A., Drosten, C., Press, W.H., and Sawyer, S.L. (2019). A metaanalysis of bat phylogenetics and positive selection based on genomes and transcriptomes from 18 species. Proc. Natl. Acad. Sci. USA *116*, 11351–11360.

He, X., Ashbrook, A.W., Du, Y., Wu, J., Hoffmann, H.H., Zhang, C., Xia, L., Peng, Y.C., Tumas, K.C., Singh, B.K., et al. (2020). RTP4 inhibits IFN-I response and enhances experimental cerebral malaria and neuropathology. Proc. Natl. Acad. Sci. USA *117*, 19465–19474.

Irving, A.T., Rozario, P., Kong, P.S., Luko, K., Gorman, J.J., Hastie, M.L., Chia, W.N., Mani, S., Lee, B.P.-H., Smith, G.J.D., et al. (2020). Robust dengue virus infection in bat cells and limited innate immune responses coupled with positive serology from bats in IndoMalaya and Australasia. Cell. Mol. Life Sci. *77*, 1607–1622.

Jones, C.T., Patkar, C.G., and Kuhn, R.J. (2005). Construction and applications of yellow fever virus replicons. Virology *331*, 247–259.

Kane, M., Zang, T.M., Rihn, S.J., Zhang, F., Kueck, T., Alim, M., Schoggins, J., Rice, C.M., Wilson, S.J., and Bieniasz, P.D. (2016). Identification of interferon-stimulated genes with antiretroviral activity. Cell Host Microbe *20*, 392–405.

Knoops, K., Kikkert, M., Worm, S.H., Zevenhoven-Dobbe, J.C., van der Meer, Y., Koster, A.J., Mommaas, A.M., and Snijder, E.J. (2008). SARS-coronavirus replication is supported by a reticulovesicular network of modified endoplasmic reticulum. PLoS Biol. *6*, e226.

Kumar, S., Stecher, G., Li, M., Knyaz, C., and Tamura, K. (2018). MEGA X: molecular evolutionary genetics analysis across computing platforms. Mol. Biol. Evol. *35*, 1547–1549.

Kumar, S., Stecher, G., Suleski, M., and Hedges, S.B. (2017). TimeTree: a resource for timelines, Timetrees, and divergence times. Mol. Biol. Evol. *34*, 1812–1819.

Li, J., Ding, S.C., Cho, H., Chung, B.C., Gale, M., Jr., Chanda, S.K., and Diamond, M.S. (2013). A short hairpin RNA screen of interferon-stimulated genes identifies a novel negative regulator of the cellular antiviral response. mBio *4*, e00385–00313.

Lindenbach, B.D., and Rice, C.M. (1997). trans-Complementation of yellow fever virus NS1 reveals a role in early RNA replication. J. Virol. *71*, 9608–9617.

Lindenbach, B.D., and Rice, C.M. (2003). Molecular biology of flaviviruses. Adv. Virus Res. *59*, 23–61.

Marukian, S., Jones, C.T., Andrus, L., Evans, M.J., Ritola, K.D., Charles, E.D., Rice, C.M., and Dustin, L.B. (2008). Cell culture-produced hepatitis C virus does not infect peripheral blood mononuclear cells. Hepatology *48*, 1843–1850.

Mitchell, P.S., Patzina, C., Emerman, M., Haller, O., Malik, H.S., and Kochs, G. (2012). Evolution-guided identification of antiviral specificity determinants in the broadly acting interferon-induced innate immunity factor MxA. Cell Host Microbe *12*, 598–604.

Naito, Y., Hino, K., Bono, H., and Ui-Tei, K. (2015). CRISPRdirect: software for designing CRISPR/Cas guide RNA with reduced off-target sites. Bioinformatics *31*, 1120–1123.

Olival, K.J., Hosseini, P.R., Zambrana-Torrelio, C., Ross, N., Bogich, T.L., and Daszak, P. (2017). Host and viral traits predict zoonotic spillover from mammals. Nature *546*, 646–650.

Pavlovich, S.S., Lovett, S.P., Koroleva, G., Guito, J.C., Arnold, C.E., Nagle, E.R., Kulcsar, K., Lee, A., Thibaud-Nissen, F., Hume, A.J., et al. (2018). The Egyptian rousette genome reveals unexpected features of bat antiviral immunity. Cell *173*, 1098–1110.e18.

Richardson, R.B., Ohlson, M.B., Eitson, J.L., Kumar, A., McDougal, M.B., Boys, I.N., Mar, K.B., De La Cruz-Rivera, P.C., Douglas, C., Konopka, G., et al. (2018). A CRISPR screen identifies IFI6 as an ER-resident interferon effector that blocks Flavivirus replication. Nat. Microbiol. *3*, 1214–1223.

Robinson, M.D., McCarthy, D.J., and Smyth, G.K. (2010). edgeR: a Bioconductor package for differential expression analysis of digital gene expression data. Bioinformatics *26*, 139–140.

Saeedi, B.J., and Geiss, B.J. (2013). Regulation of Flavivirus RNA synthesis and capping. Wiley Interdiscip. Rev. RNA *4*, 723–735.

Saito, H., Kubota, M., Roberts, R.W., Chi, Q., and Matsunami, H. (2004). RTP family members induce functional expression of mammalian odorant receptors. Cell *119*, 679–691.

Sanjana, N.E., Shalem, O., and Zhang, F. (2014). Improved vectors and genome-wide libraries for CRISPR screening. Nat. Methods *11*, 783–784.

Sawyer, S.L., Wu, L.I., Emerman, M., and Malik, H.S. (2005). Positive selection of primate TRIM5alpha identifies a critical species-specific retroviral restriction domain. Proc. Natl. Acad. Sci. USA *102*, 2832–2837.

Schoggins, J.W., Dorner, M., Feulner, M., Imanaka, N., Murphy, M., Ploss, A., and Rice, C.M. (2012). Dengue reporter viruses reveal viral dynamics in interferon receptor-deficient mice and sensitivity to interferon effectors in vitro. PNAS *109*, 14610–14615.

Schoggins, J.W., MacDuff, D.A., Imanaka, N., Gainey, M.D., Shrestha, B., Eitson, J.L., Mar, K.B., Richardson, R.B., Ratushny, A.V., Litvak, V., et al. (2014). Pan-viral specificity of IFN-induced genes reveals new roles for cGAS in innate immunity. Nature *505*, 691–695.

Schoggins, J.W., Wilson, S.J., Panis, M., Murphy, M.Y., Jones, C.T., Bieniasz, P., and Rice, C.M. (2011). A diverse range of gene products are effectors of the type I interferon antiviral response. Nature *472*, 481–485.

Schwarz, M.C., Sourisseau, M., Espino, M.M., Gray, E.S., Chambers, M.T., Tortorella, D., and Evans, M.J. (2016). Rescue of the 1947 Zika virus prototype strain with a Cytomegalovirus promoter-driven cDNA clone. mSphere, e00246-16.

Shaw, A.E., Hughes, J., Gu, Q., Behdenna, A., Singer, J.B., Dennis, T., Orton, R.J., Varela, M., Gifford, R.J., Wilson, S.J., and Palmarini, M. (2017). Fundamental properties of the mammalian innate immune system revealed by multispecies comparison of type I interferon responses. PLoS Biol. *15*, e2004086.

Simmonds, P., Becher, P., Bukh, J., Gould, E.A., Meyers, G., Monath, T., Muerhoff, S., Pletnev, A., Rico-Hesse, R., Smith, D.B., et al. (2017). ICTV virus taxonomy profile: Flaviviridae. J. Gen. Virol. *98*, 2–3.

Suzuki, Y., Chin, W.X., Han, Q., Ichiyama, K., Lee, C.H., Eyo, Z.W., Ebina, H., Takahashi, H., Takahashi, C., Tan, B.H., et al. (2016). Characterization of RyDEN (C19orf66) as an interferon-stimulated cellular inhibitor against dengue virus replication. PLoS Pathog. *12*, e1005357.

Szretter, K.J., Balish, A.L., and Katz, J.M. (2006). Influenza: propagation, quantification, and storage. Curr. Protoc. Microbiol. *29*, 15G.1.1–15G.1.24.

van den Hurk, A.F., Smith, C.S., Field, H.E., Smith, I.L., Northill, J.A., Taylor, C.T., Jansen, C.C., Smith, G.A., and Mackenzie, J.S. (2009). Transmission of Japanese encephalitis virus from the black flying fox, Pteropus alecto, to Culex annulirostris mosquitoes, despite the absence of detectable viremia. Am. J. Trop. Med. Hyg. *81*, 457–462.

Van Valen, L. (1973). A new evolutionary law. Evol. Theor. *1*, 1–30.

Wang, X., Xuan, Y., Han, Y., Ding, X., Ye, K., Yang, F., Gao, P., Goff, S.P., and Gao, G. (2019). Regulation of HIV-1 gag-pol expression by shiftless, an inhibitor of programmed −1 ribosomal frameshifting. Cell *176*, 625–635.e14.

White, M.D., Milne, R.V., and Nolan, M.F. (2011). A molecular toolbox for rapid generation of viral vectors to up- or down-regulate neuronal gene expression in vivo. Front. Mol. Neurosci. *4*, 8.

Xie, J., Li, Y., Shen, X., Goh, G., Zhu, Y., Cui, J., Wang, L.F., Shi, Z.L., and Zhou, P. (2018). Dampened STING-dependent interferon activation in bats. Cell Host Microbe *23*, 297–301.e4.

Yang, Z. (1993). Maximum-likelihood estimation of phylogeny from DNA sequences when substitution rates differ over sites. Mol. Biol. Evol. *10*, 1396–1401.

Yang, Z. (2007). PAML 4: phylogenetic analysis by maximum likelihood. Mol. Biol. Evol. *24*, 1586–1591.

Zhang, G., Cowled, C., Shi, Z., Huang, Z., Bishop-Lilly, K.A., Fang, X., Wynne, J.W., Xiong, Z., Baker, M.L., Zhao, W., et al. (2013). Comparative analysis of bat genomes provides insight into the evolution of flight and immunity. Science *339*, 456–460.

Zhou, P., Tachedjian, M., Wynne, J.W., Boyd, V., Cui, J., Smith, I., Cowled, C., Ng, J.H., Mok, L., Michalski, W.P., et al. (2016). Contraction of the type I IFN locus and unusual constitutive expression of IFN-alpha in bats. Proc. Natl. Acad. Sci. USA *113*, 2696–2701.

## STAR★METHODS

### KEY RESOURCES TABLE

| REAGENT or RESOURCE | SOURCE | IDENTIFIER |
|---|---|---|
| Antibodies | | |
| HA (Mouse) | BioLegend | 901502 |
| HA (Rabbit) | Cell Signaling Technologies | 3724S |
| WNV NS5 (Rabbit) | GeneTex | GTX131961 |
| WNV NS3 (Rabbit) | GeneTex | GTX131955 |
| WNV NS5 (Mouse) | Susan Wong | 127-215 |
| WNV NS3 (Mouse) | Susan Wong | 130-175 |
| dsRNA | SciCons | J2 |
| Flavivirus E | BioXCell | D1-4G2-4-15 |
| AF488 WGA | Invitrogen | W11261 |
| ACTB | Abcam | ab6276 |
| ACTB-HRP | Sigma | A3854 |
| KDEL (Rabbit) | Abcam | ab176333 |
| MX1 | CUSABIO | CSB-PA015249LA01HU |
| Calnexin | Enzo | ADI-SPA-860-D |
| STAT1 | Abcam | ab92506 |
| TagRFP | Evrogen | AB233 |
| IRDye 800CW Goat anti-Rabbit IgG Secondary Antibody | LI-COR | 926-32211 |
| IRDye 680RD Goat anti-Mouse IgG Secondary Antibody | LI-COR | 926-68070 |
| Goat anti-Rabbit IgG (H+L) Highly Cross-Adsorbed Secondary Antibody, Alexa Fluor 647 | ThermoFisher | A-21245 |
| Yellow Fever Virus Antibody (0G5) | Novus | NB100-64510 |
| Goat-anti-mouse IgG (H+L) Cross-Adsorbed Secondary Antibody, Alexa Fluor 647 | ThermoFisher | A-21235 |
| Anti-Coronavirus Group Antigen Antibody | Millipore | MAB9013 |
| Rb IgG Isotype | Abcam | 27478 |
| Goat-anti-Rabbit HRP | Pierce | 31460 |
| Goat-anti-Mouse HRP | Pierce | 31430 |
| Goat-anti-Mouse Alexa Fluor 555 | ThermoFisher | A21425 |
| Goat-anti-Rabbit Alexa Fluor 555 | ThermoFisher | A21430 |
| Goat-anti-Mouse Alexa Fluor 488 | ThermoFisher | A11001 |
| Goat-anti-Rabbit Alexa Fluor 488 | ThermoFisher | A11034 |
| Goat-anti-Mouse Alexa Fluor 647 | ThermoFisher | A21235 |
| Goat-anti-Rabbit Alexa Fluor 647 | ThermoFisher | A21245 |
| Bacterial and Virus Strains | | |
| EAV-GFP (Bucyrus) | Eric Snijder | N/A |
| ONNV-GFP (SG650) | Stephen Higgs | N/A |
| VEEV-GFP (TC83) | Ilya Frolov | N/A |
| PIV3-GFP (JS) | Peter Collins | N/A |
| YFV17D-Venus | Charles Rice | N/A |
| HCV-Ypet | Charles Rice | N/A |

(*Continued on next page*)

*Continued*

| REAGENT or RESOURCE | SOURCE | IDENTIFIER |
|---|---|---|
| CVB-GFP (myocarditic variant of Woodruff strain) | J. Lindsay Whitton | N/A |
| WNV-GFP (TVP 8533) | Charles Rice | N/A |
| ZIKV (PRVABC59) | CDC | KU501215 |
| HCV-GLuc (Jc1FLAG(p7-nsGluc2A)) | Charles Rice | N/A |
| VSV-GFP | Jack Rose | N/A |
| IAV (A/WSN/33) | Adolfo Garcia-Sastre | N/A |
| WNV (TX-02) | Ilya Frolov | N/A |
| ZIKV-GFP (MR766) | Matthew Evans | N/A |
| YFV-17D | Charles Rice | N/A |
| DENV (Serotype 2, strain 16681, bearing a L52F mutation in NS4B) | Charles Rice | N/A |
| HSV-1 (17) | David Leib | N/A |
| HCoV-OC43 | ATCC | VR-1558 |
| ENTV | ATCC | VR-378 |
| Chemicals, Peptides, and Recombinant Proteins | | |
| Universal Type I IFN | PBL | 11200 |
| SCR7 pyrazine | Tocris | 5342 |
| Ribonuclease H | Promega | M4281 |
| Micrococcal Nuclease | NEB | M0247S |
| RNasin Plus | Promega | N2615 |
| DNase I | NEB | M0303S |
| Random Hexamers | ThermoFisher | N8080127 |
| Pierce Protein A Magnetic Beads | ThermoFisher | 88845 |
| SuperScript IV RT | ThermoFisher | 18090050 |
| Qiashredder | Qiagen | 79654 |
| Proteinase K | ThermoFisher | AM2546 |
| iTaq Universal Sybr Green Supermix | BioRad | 1725121 |
| MuMLV RT | NEB | M0253L |
| Renilla Luciferase Assay System | Promega | E2820 |
| Pierce Anti-HA Magnetic Beads | ThermoFisher | 88837 |
| Prolong Diamond Antifade Mountant with Dapi | ThermoFisher | P36971 |
| Platinum SuperFi PCR Master Mix | ThermoFisher | 12358010 |
| Protein A Magnetic Beads | Pierce | 88845 |
| Wheat Germ Agglutinin, Alexa Fluor 488 conjugate | ThermoFisher | W11261 |
| Critical Commercial Assays | | |
| CloneMiner II | ThermoFisher | A11180 |
| Alexa Fluor 594 Tyramide SuperBoost Kit | ThermoFisher | B40942 |
| Duolink In Situ Red Starter Kit Mouse/ Rabbit | Sigma | DUO92101-1KT |
| Deposited Data | | |
| *P. alecto* RTP4 cDNA sequence | This paper | NCBI: MT955625 |
| *R. aegyptiacus* RTP4 cDNA sequence | This paper | NCBI: MT955626 |
| *T. brasiliensis* RTP4 cDNA sequence | This paper | NCBI: MT955627 |
| Experimental Models: Cell Lines | | |
| Huh7.5 | C. Rice | N/A |
| BHK-21J | C. Rice | N/A |

(*Continued on next page*)

*Continued*

| REAGENT or RESOURCE | SOURCE | IDENTIFIER |
|---|---|---|
| MDCK | C. Rice | N/A |
| HEK293T | C. Rice | N/A |
| STAT1-/- Fibroblasts | J.-L. Casanova | N/A |
| PaKiT03 | Lin-Fa Wang, G. Crameri | N/A |
| PK15 | L. Enquist | N/A |
| RO6E | DSMZ | ACC 756 |
| U2OS | ATCC | HTB-96 |
| HCT-8 | ATCC | CCL-24 |
| Tb 1 Lu | ATCC | CCL-88 |
| Oligonucleotides | | |
| See Data S3 for oligonucleotide sequences. | | N/A |
| Recombinant DNA | | |
| pHelper | Cell BioLabs | N/A |
| pAAV-DJ | Cell BioLabs | N/A |
| pAAV-Gateway | Addgene | 32671 |
| pTRIP.CMV.IVSb.ires.TagRFP | Schoggins et al., 2011 | N/A |
| pSCRPSY | Paul Bieniasz | N/A |
| pSCRBBL | Richardson et al., 2018 | N/A |
| pLentiCRISPRv2-Puro | Addgene | 98290 |
| pLentiCRISPRv2-Blast | Addgene | 98293 |
| pUC57-KAN | Genewiz | N/A |
| pVSV-Glycoprotein | Charles Rice | N/A |
| pGag-Pol | Charles Rice | N/A |
| Software and Algorithms | | |
| GraphPad Prism 8 | GraphPad Software | https://www.graphpad.com/scientific-software/prism/ |
| FlowJo v9 | BD | https://www.flowjo.com/ |
| Fiji | ImageJ | https://imagej.nih.gov/ij/ |
| R (Version 3.6.1) | The R Foundation | https://www.r-project.org/ |
| R Studio (1.2.1335) | RStudio, Inc. | https://rstudio.com/ |
| PAML | Yang, 2007 | http://abacus.gene.ucl.ac.uk/software/paml.html |
| MegaX | Kumar et al., 2018 | Megasoftware.net |
| CRISPRdirect | Naito et al., 2015 | https://crispr.dbcls.jp/ |
| Dendextend R package | Galili, 2015 | https://cran.r-project.org/web/packages/dendextend/index.html |
| Fluoview Viewer | Olympus | https://www.olympus-lifescience.com/en/support/downloads/ |
| Gblocks | Castresana, 2000 | http://molevol.cmima.csic.es/castresana/Gblocks_server.html |
| ALTER | Glez-Peña et al., 2010 | http://sing.ei.uvigo.es/ALTER/ |
| FastML | Ashkenazy et al., 2012 | http://fastml.tau.ac.il/ |
| STAR (v2.5.3) | Dobin et al., 2013 | https://github.com/alexdobin/STAR |
| edgeR | Robinson et al., 2010 | N/A |
| fastqc (0.11.2) | Babraham Bioinformatics | http://www.bioinformatics.babraham.ac.uk/projects/fastqc |
| fastq_screen | Babraham Bioinformatics | http://www.bioinformatics.babraham.ac.uk/projects/fastq_screen |
| Adobe Illustrator CS6 | Adobe Inc. | N/A |
| Figtree V1.4.4 | Andrew Rambaut | http://tree.bio.ed.ac.uk/software/figtree/ |

(*Continued on next page*)

*Continued*

| REAGENT or RESOURCE | SOURCE | IDENTIFIER |
|---|---|---|
| Other | | |
| S1000 Flow Cytometer | Stratedigm | N/A |
| A600 96-w Plate Reader | Stratedigm | N/A |
| XS3 LB 960 luminometer | Berthold | N/A |
| FV10i-LIV Laser-Scanning Confocal Microscope | Olympus | N/A |
| Zeiss Observer Z.1 | Zeiss | N/A |

## RESOURCE AVAILABILITY

### Lead Contact

Further information and requests for resources and reagents should be directed to and will be fulfilled by the Lead Contact, John Schoggins (John.Schoggins@UTSouthwestern.edu).

### Materials Availability

Cell lines and plasmids generated in this study are available upon request.

### Data and Code Availability

Original/source data for the current study are available from the Lead Contact on request. Corrected RTP4 sequences generated in this study have been deposited with the NCBI. The accession number for the *P. alecto* RTP4 sequence is Genbank:MT955625, the *R. aegyptiacus* RTP4 sequence is Genbank:MT955626, and the *T. brasiliensis* RTP4 sequence is Genbank:MT955627.

## EXPERIMENTAL MODEL AND SUBJECT DETAILS

### Cell Culture

Huh7.5 (Male), HEK-293T (Female), U2OS (Female), and MDCK (Female) cells were maintained in DMEM supplemented with 10% FBS. STAT1$^{-/-}$ fibroblasts (Female) were maintained in RPMI supplemented in 10% FBS. BHK-21J (Male) cells were maintained in MEM supplemented with 10% FBS. PaKi (Male) and RO6E (sex unknown) cells were maintained in DMEM/F12 supplemented with 10% or 5% FBS, respectively. HCT-8 (Male) cells were maintained in RPMI supplemented with 10% horse serum. PK15 (Male) and Tb 1 Lu (Female) cells were maintained in MEM supplemented with sodium pyruvate and 10% FBS. All cells were cultured at 37°C in 5% CO2. Stable cell lines were maintained by passaging in the presence of 4μg/mL puromycin (Huh7.5, STAT1$^{-/-}$ fibroblasts, PaKi) or 15μg/mL blasticidin (Huh7.5).

### Viruses

The generation and propagation of the following viruses have been previously described: EAV-GFP, ONNV-GFP, PIV3-GFP, YFV17D-Venus, HCV genotype 2a intragenotypic chimera expressing Ypet GFP (HCV-Ypet), CVB-GFP, WNV-GFP, and ZIKV strain PRVABC59 (Schoggins et al., 2011, 2014; Hanners et al., 2016). Infectious HCV-GLuc was generated from the infectious clone Jc1FLAG(p7-nsGluc2A) as previously described (Marukian et al., 2008). VSV-GFP was produced by passaging in BHK cells. IAV (A/WSN/33) was produced by inoculation of sub-confluent MDCK cells as previously described (Szretter et al., 2006). An infectious clone of non-reporter WNV (strain TX02) was kindly provided by I. Frolov (University of Alabama Birmingham) and the virus was propagated as described for WNV-GFP. A ZIKV MR766-GFP infectious clone (kindly provided by M. Evans, Icahn School of Medicine at Mount Sinai) was used to generate the virus as described (Schwarz et al., 2016). The infectious clone pACNR-FLYF-17Dx (kindly provided by C. Rice) was used to generate non-reporter YFV-17D as previously described (Richardson et al., 2018). VEEV-GFP (strain TC83, a kind gift of I. Frolov) was generated by passaging in BHK-21J cells. VSV (kindly provided by Jack Rose) was generated by passaging in BHK-21J cells. ENTV (ATCC VR-378) was produced by passaging in BHK-21J cells. DENV (serotype 2 strain 16681, bearing a L52F mutation in NS4B) was propagated as previously described (Schoggins et al., 2012). HSV-1: (a kind gift of David Leib) was produced by passaging in VeroE6 cells. Human coronavirus OC43 (ATCC strain VR-1558) was propagated in HCT-8 cells as specified by the ATCC. Viral titers were determined by antibody staining (MAB9012, Millipore) and flow cytometry. All viral stocks were clarified by centrifugation, aliquotted, and stored at -80°C until use.

## METHOD DETAILS

### Lentiviral Pseudoparticle Production and Transductions

All lentiviral pseudoparticles were generated by co-transfecting sub-confluent 293T cells with expression plasmids [pTRIP.CMV.IVS-b.ISG.ires.TagRFP (Schoggins et al., 2011), pSCRPSY (Kane et al., 2016), pSCRBBL (Richardson et al., 2018), or pLentiCRISPRv2

(Sanjana et al., 2014)], HIV-1 *gag-pol*, and VSV-glycoprotein at a ratio of 5:4:1 (TRIP), 25:5:1 (SCRPSY, SCRBBL), or 10:5:7 (Lenti-CRISPR) using XtremeGene 9 (Roche). Two to six hours post-transfection, media was replaced with DMEM containing 3% FBS. Supernatants were collected at 48h and 72h, pooled, filtered with a 0.45μM filter, supplemented with 20mM HEPES, aliquotted, and stored at -80°C until use.

Cells were either transduced by passive infection or by spinoculation. Briefly, lentivirus was added to a minimum volume of transduction media (3% FBS, appropriate base media for each cell line, 4μg/mL polybrene, 20mM HEPES) and added to cells. For passive transductions, cells were allowed to rest with pseudoparticle-containing media for 1-2 hours before addition of complete medium. For spinoculations, cells were centrifuged at 800xg at 37°C for 40 minutes, after which media was replaced with standard growth media.

### AAV Production

AAV-DJ was produced with the helper-free AAV-DJ system (CellBioLabs). Briefly, pHelper, pAAV-DJ, and pAAV-Gateway expression cassettes were transfected with XtremeGene9 into subconfluent 293T cells at a ratio of 1:1:1. 48h post-transfection, supernatant and lifted cells were combined, freeze-thawed four times in a dry ice/ethanol bath, centrifuged to clear debris, aliquotted, and stored at -80C until use. The pAAV-Gateway cassette, a kind gift from Matthew Nolan (Addgene# 32671) (White et al., 2011), was packaged for gene expression. AAV titers were determined by qPCR with ITR-specific primers.

### CRISPR Editing

*RTP4* KO clonal PaKi cell lines: PaKi cells were seeded at 250,000 c/w on a 6w plate. Cells were transfected the following day with LentiCRISPRv2 plasmid containing guide specific to *RTP4* using lipofectamine. 48h post-transfection cells were replated into puromycin (4μg/mL) selective media. After two days, selective media was replaced with complete non-selective media. Cells were plated in limiting dilutions and single-cell clones were expanded and targeted clones were identified by Sanger sequencing.

*STAT1* KO cells: PaKi cells were seeded at 250,000 c/w on a 6w plate. Cells were transduced with lentiviral pseudoparticles containing a CRISPR guide specific to *STAT1*. 48h post-transduction cells were replated into puromycin (4μg/mL) selective media. Following selection, cells were plated in limiting dilutions and single-cell clones were expanded and targeted clones were identified by western blotting.

Dual-guide U2OS cells: U2OS cells were co-transduced with lentiviral pseudoparticles containing two separate guides specific to human *RTP4* from the Brunello library (Broad Institute) under either a puromycin or a blasticidin selection cassette. The bulk population of cells was passaged in selective media (1μg/mL puromycin and 10μg/mL blasticidin) for one week and then maintained in lower-concentration selective media (0.5μg/mL puromycin and 5μg/mL blasticidin).

Dual-guide PK15 cells: PK15 cells were co-transduced with lentiviral pseudoparticles containing two separate guides specific to pig *RTP4* under either a puromycin or a blasticidin selection cassette. The bulk population of cells was passaged in selective media.

Genomically Tagged HA-RTP4 cells: PaKi cells were seeded at 250,000 c/w on a 6w plate. Cells were transfected the next day with a 2:1 ratio of an HA-tagged homology arm and LentiCRISPRv2 plasmid containing a guide specific to RTP4 using Lipofectamine 3000 (Invitrogen) in the presence of 0.1μm SCR-7, a DNA ligase IV inhibitor (Tocris). 72h post-transfection cells were replated into puromycin (4μg/mL) selective media. After three days, selective media was replaced with complete non-selective media. Cells were plated in limiting dilutions and single-cell clones were expanded. Targeted cells were identified by PCR and validated by Sanger sequencing and western blotting.

### Transfection of PaKi Cells

PaKi cells were transfected with Lipofectamine 3000 (ThermoFisher) per manufacturer protocols. For cells seeded on a 24w plate, cells 500ng of plasmid was mixed with 25μl of Optimem and 1μl of p3000 reagent. This mixture was added to premixed Lipofectamine (1.5μl) and Optimem (25μl). After ten minutes, 50μl of the transfection complex was added to each well. Mixes were scaled linearly with well size for transfections on other formats, and master mixes were made when appropriate.

### Viral Infections

Cells were seeded at 50,000-100,000 (24w plate),150,000-200,000 (12w plate), 4,000,000 (10cm dish), or 12,000,000 (15cm dish) cells per well, depending upon experiment endpoint, the day prior to infection. Virus was added to cells in a minimal volume and incubated for one hour (all viruses besides DENV) or two hours (DENV). After incubation, complete media was added to maintain cells until harvest. Unless specifically stated, all infections were performed at an MOI $\leq$ 1 infectious units per cell to ensure that most cells were infected by only one viral particle. All infected cells were incubated at 37C with the exception of HCoV-OC43, which was incubated at 33C. For infections to assess viral production by plaque assay, inoculum was aspirated and cells were washed four times with PBS prior to addition of complete media. Unless specifically mentioned in the figure legend, infectivity for experiments is quantified by flow cytometry. All WNV infections were performed in a Biosafety Level 3 (BSL3) facility according to institutional guidelines provided by the UT Southwestern Office of Business and Safety Continuity.

### Plaque Assays

For WNV, ENTV, and YFV plaque assays, BHK-21J cells were seeded at 400,000 cells per well on 6 well plates one day prior to infection. Supernatants were serially diluted in MEM supplemented with 1% FBS and 200ul of relevant dilutions were applied to BHKs.

Cells were incubated with intermittent rocking for one hour, after which wells were overlaid with overlay media (1% Avicel, DMEM, 4% FBS, 100U/mL penicillin/100μg/mL streptomycin, 10mM HEPES, 0.1%$NaHCO_3$). After three days, wells were fixed with formaldehyde and plaques were visualized by staining with crystal violet.

### Crystal Violet Stains

To assess cell survival, cells were fixed by direct addition of formaldehyde to culture media to a final concentration of 2% and subsequently stained with crystal violet. Images of crystal violet stains were captured using a Google Pixel 2 smartphone.

### Intracellular Antibody Staining for Flow Cytometry

Intracellular staining was performed using the CytoFix/Cytoperm Solution Kit (BD). Briefly, cells were fixed/permeabilized for 30 minutes, washed once, incubated in primary antibody (4G2: 1:2500, 0G5: 1:2000, 542-7D: 1:500, MAB8251: 1:1000) for 30 minutes, washed once, incubated with secondary antibody for 30 minutes, washed once, and resuspended in FACS buffer (PBS plus 3% FBS). Viral proteins used for assessing viral infection: E protein (4G2 (BioXCell): DENV, ZIKV, WNV, ENTV; 0G5 (Novus): YFV), N protein (542-7D (Millipore-Sigma): HCoV-OC43), NP (MAB8251 (Millipore-Sigma): IAV).

### Flow Cytometry

Samples were run in a Stratedigm S1000 flow cytometer with a A600 96-well plate reader. When necessary, compensation was performed at the time of collection in CellCapture (Stratedigm). FlowJo (BD) was used to quantify data.

### Digitonin Membrane Association Assays

For immunofluorescence: cells were washed once with PBS, washed once with HCN buffer (50mM HEPES, 150mM $NaCl_2$, 2mM $CaCl_2$), then either mock treated or permeabilized with 20μM digitonin in 250μl HCN for 15 minutes at RT, washed once with PBS, and fixed with PFA. Standard immunofluorescence was used to detect protein.

For western blotting: 100,000 cells were washed once with PBS, and once with HCN. Cells were resuspended in 100μl of HCN supplemented with 20μM digitonin (or mock) and incubated for 20 minutes at 4C with end-over-end rotation. Cells were pelleted, supernatant was removed and combined with 2X SDS loading buffer, and pellets were washed once with 500μl of HCN buffer. Pellets were resuspended in SDS loading buffer.

### CLIP-qPCR

CLIP experiments were performed as previously described with slight modification (Conrad, 2008). Briefly, cells were washed with PBS and cross-linked with 150mJ/$cm^2$ in a Spectrolinker XL1000 or XL1500 (Spectroline). Cells were scraped, pelleted, and snap-frozen. Cells were thawed and lysed in SDS lysis buffer (0.5% SDS, 50mM Tris-Cl pH 6.8, 1mM EDTA, 0.125mg/mL heparin, 2.5mg/mL torula yeast RNA (Sigma), and 1x protease inhibitors (Roche)). Samples were boiled at 65C for 5 minutes and returned to ice. Buffer was adjusted to RIPA by addition of a correction buffer (1.25%NP-40, 0.625% sodium deoxycholate, 62.5mM Tris-HCl pH 8.0, 2.25mM EDTA, 187.5mM NaCl). Lysate was passed through a QIAshredder (Qiagen) twice (10cm plates) or three times (15cm plates). Lysates were cleared by three high-speed spins with tube transfers. Cleared lysates were supplemented with 5mM $CaCl_2$ and treated with 30U of DNase (NEB) for 15 minutes. When performed, nuclease digestion was completed by addition of 50 gel units of micrococcal nuclease for ten minutes, which was then quenched by addition of EGTA to a final concentration of 20mM. RIPA buffer (1%NP-40, 0.5% sodium deoxycholate, 0.1% SDS, 150mM NaCl, 50mM Tris-Cl pH 8.0, 2mM EDTA). Antibody conjugated beads (preconjugated HA or 10ug of antibody/protein A-conjugated beads) were added to samples (Pierce). Samples were rotated end over end at 4C for 2h. Samples were placed on a magnetic separator and washed three times with RIPA, once with RIPA supplemented with 1M Urea, and twice with RIPA. RNA was eluted from beads by addition of Proteinase K buffer (0.5mg/mL Proteinase K (Ambion), 0.5% SDS, 20mM Tris-Cl pH 7.5, 5mM EDTA, 16.7ng/μl GlycoBlue (Invitrogen), 0.1mg/mL torula yeast RNA) and incubation for 1-2h with shaking at 37C. Following elution, RNA was extracted with phenol-chloroform-isoamyl alcohol, extracted with chloroform, precipitated, DNase-treated, re-purified, and cDNA was generated using Superscript IV and random hexamers. cDNA was treated with RNase H and RNase A, precipitated, and resuspended in a low volume of water for storage at -20C. cDNA was diluted prior to qPCR.

### Polysome Profiling

Cycloheximide was added to culture media to a final concentration of 100ug/mL and cells were incubated on ice for five minutes to fix ribosomes to RNA. Media was aspirated and cells were resuspended in 500μl of Polysome extraction buffer (140mM KCl, 5mM $MgCl_2$, 20mM Tris-HCl pH 8.0, 1mM DTT, 100ug/mL cycloheximide). Cells were pelleted and resuspended in 200μl of PEB + 1% Triton-X100. Cells were incubated on ice for 20 minutes with intermittent tipping. Lysates were cleared by centrifugation (10,000xg, 10m, 4C) and transferred to a fresh tube. 10 OD 260 of lysate was resolved on a 5mL gradient (50% w/v to 12.5% w/v sucrose in PEB) by centrifugation for 150,000xg for 1.5h in an SW40ti rotor. Following centrifugation, the bottom of the tube was pierced and 500μl fractions were collected. Polysome-containing fractions were identified by spectroscopy, and both polysome-associated and input RNA were isolated with TRIzol (Invitrogen) and cDNA was synthesized using Mu-MLV RT (NEB).

### Quantitative RT-PCR

For most experiments, RNA was isolated using TRIzol (Invitrogen) and cDNA was reverse-transcribed using MμLV reverse transcriptase (NEB). RT-qPCR reactions were performed using iTaq Universal SYBR Green Supermix (Bio-Rad). For some gene expression assays and the viral cold-bind experiment, one-step reverse transcriptase pPCR was performed using the QuantiFast SYBR Green RT-PCR kit (Qiagen).

### Immunofluorescence

Cells were fixed with 4% PFA in PBS. Cells were washed with PBS, then permeabilized with 0.2% Triton-X 100. Cells were blocked with 10%BSA/5%Goat Serum/PBS for at least 30 minutes. Primary antibody was added in blocking solution and incubated for 1-2 hours. Cells were washed 3x with PBS, after which secondary antibody was added in 3% BSA and incubated for 30 minutes. When included, wheat germ agglutinin was added to the secondary antibody dilution. Cells were washed 3x with PBS, and then mounted using ProLong Diamond (ThermoFisher). Imaging was performed either on an Olympus FV10i-LIV or a Zeiss Observer Z.1. Images were processed in ImageJ or Fluoview Viewer (Olympus).

### Tyramide Signal Amplification

The Tyramide SuperBoost system (ThermoFisher) was used per manufacturer specifications with a labeling time of five minutes. Cells were subsequently counterstained by standard immunofluorescence.

### Proximity Ligation Assay

The DuoLink proximity ligation assay system (Sigma) was used per manufacturer protocol. Briefly, cells were fixed with 4% PFA, washed, and blocked. Primary antibodies were incubated for two hours, after which cells were washed twice and incubated with anti-mouse and anti-rabbit probes for one hour. After two washes, adapters were ligated and rolling circle amplification was performed. Following final washes, slides were mounted with DuoLink mounting media with DAPI and immediately imaged. Single primary and no primary controls were included with every replicate.

### Immunoprecipitations

Cells were harvested with Accumax, pelleted, and resuspended in RSB150T (50mM TRIS-HCl 7.5, 150mM $NaCl_2$, 2.5mM MgCl2, 1mM CaCl2, 1% Triton-X100). Lysates were treated with DNase (NEB) at 20U/mL for 10 minutes, after which lysates were cleared by centrifugation at 16,000xg for 10 minutes at 4C. Lysates were subsequently incubated with equilibrated beads for one hour, after which beads were captured on a magnetic separator and washed seven times in RSB150T, including one wash with 0.1% SDS. Protein was eluted by boiling in 1x SDS buffer.

### cDNA Library Construction

PaKi cells were seeded at 2E6 cells in two 10cm dishes. The following day, cells were treated with universal Type I interferon at 100U/mL. After 6 hours, RNA was isolated with TRIol. mRNA was purified with an mRNA purification kit (Miltenyi). The CloneMiner II cDNA library construction kit (ThermoFisher) was used to generate the Gateway-compatible cDNA library from 2ug of mRNA. Library size was calculated by plating dilutions on agarose plates. The library was qualified by restriction digest to ensure appropriate average insert size (Figure S5A). The cDNA library was transferred into an expression library (pSCRPSY) by several pooled LR reactions. Libraries were amplified using SeaPrep soft agar (Lonza) per manufacturer recommendations. Briefly, 2X LB/SeaPrep agar was autoclaved and chilled to 25°C in a water bath, after which antibiotics and library-transformed bacteria were added. Inoculated LB was aliquotted into 50mL conical vials and submerged in wet ice for one hour, after which conicals were incubated at 37°C for 48h. Conicals were centrifuged, agar was decanted, and pellets were pooled and maxiprepped (Qiagen). Library statistics are included in Table S1.

### Screen for Antiviral bat cDNAs

Huh7.5 cells were transduced at an MOI of 0.5 with lentiviral pseudoparticles containing the black flying fox cDNA library (estimated transcriptome coverage: 20x) to limit the number of cells with multiple lentiviral inserts. The library was introduced at roughly 10x coverage and cells were expanded prior to infection. Library-transduced Huh7.5 cells were infected with DENV (library coverage 20x) or ZIKV (library coverage 100x) at an MOI of 0.01. RNA was harvested from cells at 14 days (ZIKV) and 31 days (DENV) post-infection. RNA from surviving cells was compared to RNA from uninfected, library-transduced cells (10x coverage) to identify enriched cDNAs.

### Plasmids and Cloning

*RTP4* orthologs were cloned from oligo(dT)-primed cDNA from IFN-treated cells as follows: Egyptian fruit bat, RO6E cells; dog, MDCK cells; Mexican free-tailed bat, Tb 1 Lu cells; pig, PK15 cells, using gene-specific primers. Black flying fox *RTP4* was cloned from the black flying fox cDNA library generated in this work using gene-specific primers. Human *RTP4* and *IRF1* were previously cloned (Schoggins et al., 2011). Rhesus macaque *RTP4* was previously cloned (Kane et al., 2016). Mouse *RTP4* was synthesized as a gBlock (IDT). Cow *RTP4* was cloned from the Mammalian Gene Collection clone ID 8120985 (Dharmacon) using gene-specific

PCR primers. Reconstructed ancestral mammalian *RTP4* was synthesized (IDT). Black flying fox *IFI6* was synthesized (Genewiz). Black flying fox *SHFL* was cloned from the black flying fox cDNA library generated in this work using gene-specific primers.

The following orthologs were HA-tagged by restriction digest and ligation of annealed HA oligos: cow, black flying fox, rhesus macaque, human, Egyptian fruit bat. HA tags were integrated into the cloning primers for mouse, Mexican free-tailed bat, pig, dog, and ancestral reconstructed *RTP4*.

Serial truncations of black flying fox *RTP4* were cloned by PCR using primers listed in Table S3. Black flying fox *RTP4* ZFD point mutations were cloned by restriction digest using synthesized gBlocks (IDT). Human *RTP4* ZFD point mutation was introduced using QuickChange mutagenesis.

A doxycycline-inducible RTP4 expression construct was generated by directional ligation of PCR-amplified HA-tagged paRTP4 using primers with flanking AgeI and MluI cut sites into pTRIPZ (Dharmacon).

The freetail bat RTP4 escape mutant infectious clone was generated by overlap extension PCR. Briefly, primers containing the identified point mutation (YFV17DE2057K-F, YFV17DE2057K-R) were used along with primers (10F and 11R) that flanked upstream (NheI) and downstream (NgoMIV) cut sites to amplify fragments of the YFV genome with the desired point mutation. These fragments were purified and stitched together, and the resulting product was ligated into the parental pACNR-FLYF-17Dx plasmid.

CRISPRdirect (Naito et al., 2015) was used to design CRISPR guides for black flying fox *RTP4*, black flying fox *STAT1*, and pig *RTP4*. Human *RTP4* guides were generated based on the Brunello Library (Broad). CRISPR guides were cloned into LentiCrisprV2 as previously described (Sanjana et al., 2014). pUC57-KAN-HApaRTP4locus (the donor vector that was used for genomic tagging) was synthesized by Genewiz.

All expression constructs were cloned into the Gateway expression vectors pSCRPSY (Kane et al., 2016), pSCRBBL (Richardson et al., 2018), pTRIP (Schoggins et al., 2011), or pAAV-Gateway by LR recombinase reactions.

All referenced primers are listed in the annotated oligo list (Data S3).

### *In Vitro* Transcription of Viral and Replicon RNA

Viral infectious clone (see: Cell Culture and Viruses) and replicon (YFV-R.luc2A-RP) (Jones et al., 2005) RNA was transcribed using the mMessage mMachine SP6 kit (Ambion). RNA was purified using either RNeasy mini kit (Qiagen) or MEGAClear (ThermoFisher).

### Electroporation of Viral RNA

Electroporations were performed as previously described (Lindenbach and Rice, 1997). Briefly, BHK-21J or STAT1$^{-/-}$ human fibroblasts were trypsinized, washed in ice-cold PBS, and 8E6 cells in 400ul of PBS were aliquotted into cuvettes along with 5μg of viral RNA. Cells were electroporated at 860V with five pulses and re-seeded into flasks or dishes for production.

### Western Blotting

Unless otherwise noted, cells were lysed directly in 1x SDS loading buffer (10% glycerol, 5% BME, 62.5mM TRIS-HCl pH 6.8, 2% SDS, and BPB), boiled, and sonicated (Sonics Vibra-Cell CV188). Samples were run on 12% TGX FastCast acrylamide gels (Bio-Rad) and transferred to nitrocellulose or PVDF membranes using a TransBlot Turbo system (Bio-Rad). Blots were blocked in 5% dry milk/TBS-T for 30 minutes to an hour at RT or overnight at 4C. Primary antibodies were diluted in 5%BSA/TBS-T and added for 1 to 2 hours at RT or overnight at 4C. Blots were washed four times in TBS-T before addition of HRP-conjugated secondary antibody in 5% milk for thirty minutes. Blots were washed four times in TBS-T prior to detection with either Pierce ECL (ThermoFisher) or Clarity ECL (Bio-Rad) substrate and exposure to radiography film. For quantitative blotting, LI-COR IRDye secondary antibodies were used and signal was detected using a LI-COR Odyssey Fc detection system.

### Replicon Assay

Cells were seeded at 35,000 cells per well in 48 well plates the day before transfection. 100ng YFRluc-2A RNA was transfected into each well using TransIT-mRNA (Mirus). Cells were washed once with PBS and lysed in Renilla lysis buffer and assayed using the Renilla Luciferase Assay System (Promega).

### HCV-GLuc Assay

Cells were seeded at 35,000 cells per well in 48 well plates the day before infection. Cells were infected with HCV-GLuc at an MOI of 0.5. Supernatants were collected and replaced with fresh media at the indicated time points. Supernatants were stored at -80C for the duration of the time course, after which they were quantified by luciferase assay using the Renilla Luciferase Assay System (Promega).

### Viral Cold Bind-qPCR Assay

PaKi cells were plated at 7E5 cells per well on a 24-well plate. The next day, cells were equilibrated to 4 °C for 30 min in growth medium. Media was then aspirated and YFV-17D diluted in cold 1% FBS/RPMI was added and incubated for 1 h at 4 °C. Cells were then washed 2 x with ice-cold PBS and harvested for RNA by RNeasy Mini Kit (Qiagen). Viral concentration was quantified by qRT-PCR. A standard curve was generated by spiking in vitro transcribed YFV-17D RNA into a background of 40 ng uninfected cellular RNA and used to back-calculate fg YFV RNA for each sample based on $C_T$ value.

### Doxycycline Induction for Viral Infections

One day after plating, media was replaced with doxycycline-containing media at indicated concentrations. 24 hours post-treatment, cells were infected as per standard protocol. After one hour, inoculum was aspirated and freshly-diluted doxycycline-containing media was added back for the duration of the infection. 50mg/mL doxycycline stocks were stored in DMSO at -20C and diluted into sterile water at a 1000x concentration, which was then added to growth media.

### Serial Passaging and Viral Sequencing

Huh7.5 cells expressing RTP4 orthologs were infected with YFV-17D, ENTV, or WNV at an MOI of 5 (ENTV, YFV) or 30 (WNV). After one (ENTV) or two (YFV and WNV) days, one-third of the supernatant was transferred to naive cells and allowed to infect for two days. Serial passaging proceeded for seven (ENTV, YFV) or 15 (WNV) passages. After validation of the YFV escape mutant, BHKs were infected with limiting dilutions of viral stocks and clonal YFV populations were derived from a dilution at which roughly 40% of challenged wells exhibited CPE. BHK-21J cells were infected with clonal YFV escape mutant viral stocks for 48h, after which RNA was extracted with TRIzol. cDNA synthesis was primed with random hexamers and RT was performed using SuperScript IV (Invitrogen). Tiling PCR was used to amplify the viral genome in roughly 1kb fragments. Sanger sequencing was used to identify mutations relative to wild-type YFV-17D.

### Phylogenetic Analysis

Multiple sequence alignments were generated using MUSCLE as implemented in MEGA X (Kumar et al., 2018). Alignments were trimmed using Gblocks (Castresana, 2000). When required, file formats were converted using ALTER (Glez-Peña et al., 2010). PAML was used to assess signatures of evolutionary pressure present in nucleic acid alignments. Briefly, CodeML was used with the F3x4 codon frequency table and default settings (Yang, 2007). Likelihood ratio tests were used to compare Model 8 (beta and omega - allowing for positive selection) and Model 7 (beta - no positive selection), as well as Model 8 and Model 8a (beta and omega, constrained to no positive selection). Sites that passed a stringent test (Bayes empirical bayes) test were considered to be undergoing positive selection. To perform a free-ratio analysis, PAML was run with Model 1 (branch) and NSsites = 0 to obtain a dN/dS value for each branch.

### Ancestral Sequence Reconstruction

An alignment of 35 mammalian *RTP4* sequences was input into FastML (Ashkenazy et al., 2012) using default parameters. The resulting sequence was synthesized (IDT).

### Clustering and Correlation Analysis of Phylogenetic, Expression, and Infectivity Data

Hierarchical clustering was used to generate dendrograms for infectivity data (normalized to vector control) and protein expression (normalized to actin) in R. The package dendextend (Galili, 2015) was used to compare clusters to a phylogenetic tree of all orthologs using the Baker's gamma statistic, a measure of the similarity of two tree topologies. R code is available upon request.

### Colocalization Analysis

Colocalization analysis was performed using coloc2 in ImageJ. When possible, individual cells or small clusters of cells were independently analyzed by defining ROIs based on bright field images.

### RNA Sequencing & Analysis

RNA Sequencing was performed by Genewiz (NextSeq 500 2x150PE configuration). Fastq files were subjected to quality check using fastqc and fastq_screen. Reads from each sample were mapped to the *Pteropus alecto* (assembly ASM32557v1) using STAR (V2.5.3) (Dobin et al., 2013). Read counts mapping uniquely to *Pteropus alecto* genes were generated using STAR and differential expression analysis was performed using edgeR (Robinson et al., 2010).

### ISG Length Comparison

RTP4 ortholog lengths were downloaded from the NCBI on 2/10/2020. Outliers were removed using the ROUT test with Q = 1. N = 72 (Mx1), 101 (Viperin), 85 (IFI6), 145 (SHFL), and 118 (RTP4).

## QUANTIFICATION AND STATISTICAL ANALYSIS

Statistical analyses were performed using GraphPad Prism unless otherwise noted. Unless otherwise indicated, all comparisons are relative to control (Ctrl), as labeled. For data with two groups, two-tailed t tests were used. For data with more than two groups, ANOVA tests were used and appropriate adjustments were made for multiple hypothesis testing. Additional details are available in all figure legends where any statistical tests were performed. Unless otherwise specified, P values are denoted as follows: n.s. not significant, *P<0.05, **P<0.01, ***P<0.001, ****P<0.0001.